


**Please cite the Published Version**

Jiang, SC, Bai, W  and Tang, GQ (2018) Numerical simulation of wave resonance in the narrow gap between two non-identical boxes. *Ocean Engineering*, 156. pp. 38-60. ISSN 0029-8018

**DOI:** <https://doi.org/10.1016/j.oceaneng.2018.02.055>

**Publisher:** Elsevier

**Version:** Accepted Version

**Downloaded from:** <https://e-space.mmu.ac.uk/620010/>

**Usage rights:**  [Creative Commons: Attribution-Noncommercial-No Derivative Works 4.0](https://creativecommons.org/licenses/by-nc-nd/4.0/)

**Additional Information:** This is an Author Accepted Manuscript provided by Elsevier of a paper in *Ocean Engineering*.

**Enquiries:**

If you have questions about this document, contact [openresearch@mmu.ac.uk](mailto:openresearch@mmu.ac.uk). Please include the URL of the record in e-space. If you believe that your, or a third party's rights have been compromised through this document please see our Take Down policy (available from <https://www.mmu.ac.uk/library/using-the-library/policies-and-guidelines>)

# Numerical simulation of wave resonance in the narrow gap between two non-identical boxes

Sheng-Chao Jiang<sup>a,b,\*</sup>, Wei Bai<sup>c</sup>, Guo-Qiang Tang<sup>d</sup>

<sup>a</sup>*School of Naval Architecture, State Key Laboratory of Structural Analysis for Industrial Equipment, Dalian University of Technology, Dalian 116024, China*

<sup>b</sup>*Collaborative Innovation Center for Advanced Ship and Deep-Sea Exploration, Shanghai 200240, China*

<sup>c</sup>*School of Computing, Mathematics and Digital Technology, Manchester Metropolitan University, Chester Street, Manchester M1 5GD, UK*

<sup>d</sup>*State Key Laboratory of Coastal and Offshore Engineering, Dalian University of Technology, Dalian 116024, China*

---

## Abstract

Wave resonance in the narrow gap between two side-by-side non-identical boxes is investigated by employing a two-dimensional numerical wave flume based on the OpenFOAM<sup>®</sup> package. The focus of this study is to examine the influence of the energy transformation and the energy dissipation on the hydrodynamic behavior of wave response around resonant conditions. Numerical simulations show that the unrealistic wave resonant responses in the narrow gap by the linear potential flow model are due to not only the energy dissipation induced by the fluid rotational motion, but also the energy transformation associated with the free surface. With the increase of incident wave amplitude, relatively more energy is reflected, leading to the decrease of wave resonant response and energy dissipation in the narrow gap at the resonant frequency. When slightly away from the resonant frequency, the energy dissipation becomes the dominant factor for the decrease of wave response in the narrow gap with increasing the incident wave amplitude. As for the influence of gap configuration, on one hand, energy dissipation has the dominant effect for the typical case of small upstream and large downstream box drafts. On the other hand, the reflected energy is more important for the typical large upstream and small downstream box drafts. More resonant fluid exists in the gap with the increase of gap breadth, leading to the decrease of reflection coefficient and the increase of transmission coefficient.

*Keywords:* Wave resonance, Narrow gap, Energy dissipation, Energy transformation, Non-identical boxes, OpenFOAM<sup>®</sup>

---

## 1. Introduction

In recent years, as the offshore oil and gas explorations and operations have moved towards deeper waters and harsher environments, Floating Production Storage and Offloading (FPSO) and Floating Liquefied Natural Gas (FLNG) production systems become more attractive. These structures are maintained stationary by a spread or turret mooring system, and a Liquefied Natural Gas (LNG) ship or shuttle tanker periodically

---

\*Corresponding author

Email address: [jiangshengchao@foxmail.com](mailto:jiangshengchao@foxmail.com) (Sheng-Chao Jiang)

6 approaches them for loading gas or oil according to a close proximity in side-by-side arrangement. For this  
7 loading operation, one of the key technical challenges is the fluid resonance in the narrow gap between them  
8 under the wave action.

9 Wave resonance in the narrow gap between two bodies in a close proximity has been studied extensively.  
10 Early examinations were focused on the theoretical study of eigenfrequency and eigenfunction of the resonant  
11 modes, based on the linearized potential flow theory. An analytical solution was derived in Molin (2001) for  
12 the barges with infinite length and beam in the infinite water depth, where the formula for the resonant  
13 frequencies of piston- and sloshing modes were obtained via solving an eigenvalue equation. Molin et al.  
14 (2002) further extended the work to the gap resonance in an open-ended narrow gap. Furthermore, Faltinsen  
15 et al. (2007) proposed an analytical method based on the domain decomposition approach, in which the  
16 piston-like mode in a two-dimensional moonpool between two heaving rectangular floating hulls in the finite  
17 water depth was discussed. Besides the analytical solutions, numerical simulations in the framework of  
18 potential flow theory have also been adopted to investigate the resonant modes, for example in Sun et al.  
19 (2010) where the free surface piston- and sloshing-modal resonant behaviour around two adjacent barges was  
20 investigated by using the second-order potential flow analysis in the frequency domain.

21 According to extensive comparisons, it has been demonstrated that the potential flow model is capable of  
22 predicting the resonant frequencies and capturing the resonant modes. However, the potential flow model was  
23 reported to over-predict the resonant amplitudes. Focused on this problem, Saitoh et al. (2006) conducted a  
24 set of experimental investigations in a wave flume, and suggested that the resonant amplitudes are dependent  
25 on the body draft and gap breadth. This conclusion is consistent with the analytical and experimental results  
26 of Molin (2001). Iwata et al. (2007) extended this work to the three-body problem, indicating that the number  
27 of boxes also has the significant effect on resonant phenomena. At the same time, with the fast development  
28 of computing technology and numerical technique, Computational Fluid Dynamics (CFD) simulation has  
29 also been taken as an alternative method in recent years. Lu, Teng, Cheng, Sun and Chen (2011); Lu, Teng,  
30 Sun and Chen (2011) investigated the variations of resonant amplitudes by a three-step high-order upwind  
31 Taylor-Galerkin Finite Element Method (FEM). In Moradi et al. (2016) the effect of water depth on resonant  
32 behavior of the fluid trapped between two side-by-side bodies was studied. Numerical results found that the  
33 potential flow model not only over-predicts the resonant wave amplitude, but also gives an incorrect variation  
34 tendency of the resonant wave amplitude with water depth.

35 In order to reduce the computational cost of fully CFD simulations, the coupling model based on the  
36 domain decompositions method has been also established. Elie et al. (2013) adopted the approach of Spectral  
37 Wave Explicit Navier-Stokes Equations (SWENSE), which is a combination of the linear potential flow model  
38 in the frequency domain and the viscous fluid model with RANS turbulent equations, to simulate the gap  
39 resonance between side-by-side barges. In addition, in the numerical simulation of Fredriksen et al. (2014),  
40 as well as the early work in Kristiansen and Faltinsen (2012), the coupling models based on the domain  
41 decomposition were adopted, in which the laminar Navier-Stokes equations were applied in the lower region

42 of the gap, while the potential flow model was used in the upper region of the gap and the outer region. This  
43 in fact acquiesces that the fluid rotational motion is important around the gap bottom, while the potential  
44 model may be enough for the free surface simulation. Generally, acceptable results of resonant amplitude  
45 can be obtained in various experimental tests and CFD simulations, however, the mechanical essence behind  
46 the hydrodynamic behavior of the resonant phenomena is still an interesting field. On one hand, it is an  
47 important academic problem on the topic of wave and multi-body interactions, which is one type of so-  
48 called 'trapped structures' in a broad sense. On the other hand, an essential understanding about the major  
49 factor on the over-prediction by potential flow models can help to develop an approximated method for the  
50 convenient use in industry.

51 It seems to be speculated that the over-predictions of wave resonance come from the ignorance of the  
52 inherent fluid viscosity in potential flow models. Based on this hypothesis, attempts to introduce some  
53 damping artificially in the linear potential flow model has been suggested. Newman (2004) modelled a  
54 damping term as the body force on the free surface between side-by-side vessels, and Chen (2004) introduced  
55 a damping force term into the free surface boundary conditions, which was explained as energy dissipation.  
56 The efficiency of the linear dissipative term was presented by Jean-Robert et al. (2006) with comparisons to  
57 the commercial software WAMIT<sup>®</sup> and HydroStar<sup>®</sup>, as well as measured data. These modified potential  
58 flow models are able to suppress unrealistic values, but still cannot capture the actual physical sense. A  
59 CFD simulation by Lu et al. (2010) suggested that the wave amplitude in the narrow gap is closely relevant  
60 to the vertical velocity along the gap bottom. Examinations of flow pattern indicated that the most violent  
61 rotational flow field happens in the vicinity of the gap entrance, where the significant vortex shedding and  
62 attached vortex structure can be observed. Faltinsen and Timokha (2015) accounted for the vortex-induced  
63 damping by quantifying a pressure discharge condition in the gap opening. The calculations can be supported  
64 by their earlier experimental and numerical data in Faltinsen et al. (2007). Lu and Chen (2012) quantitatively  
65 calculated the energy dissipation rate for the fluid resonance in the narrow gap induced by waves based on  
66 the Navier-Stokes flow solutions. It suggested that the flow separation and vortex motion play the most  
67 important role in energy dissipation for a wall bounded region. The majority of energy dissipation happens  
68 around the gap entrance, not on the free surface in the narrow gap. Similar findings were also obtained by  
69 Kristiansen and Faltinsen (2010) for the piston-mode wave resonance in the gap formed by a ship model  
70 arranged in front of a vertical wall. However, due to the existence of vortices square term in the expression  
71 of energy dissipation rate, it is not easy to compute the energy dissipation directly, and a clear relationship  
72 between energy dissipation and resonant amplitude or other parameters is not currently available.

73 In addition to the energy dissipation by the fluid viscosity, the process of energy transformation due to the  
74 large-amplitude free surface motion may also play an important role on wave resonances in the narrow gap.  
75 A fully nonlinear potential flow model was adopted by Feng and Bai (2015) for the wave resonance between  
76 two barges, in which the lateral piston mode and longitudinal sloshing mode were successfully captured. In  
77 their study, although the free surface nonlinearity was found to play a minor role in suppressing the over-

78 predicted resonance response, nonlinear analysis illustrated the gap resonance to be equivalent to a stiff spring  
79 in a nonlinear mass-spring system: the resonant frequency slightly shifts to higher values as incident wave  
80 steepness increases. This is an important process of energy transformation due to the large-amplitude piston-  
81 like free surface oscillation. Ananthakrishnan (2015) investigated the effect of viscosity and nonlinearity on  
82 the forces and waves generated by a floating twin hulls under heave oscillations. Numerical results showed  
83 that the nonlinear effect on the wave forces is significant at all frequencies for the large amplitude oscillation  
84 relative to the hull draft. Besides, the influence of interaction between the energy transformation in the free  
85 surface motion and the energy dissipation in the fluid rotational motion can be speculated during the process  
86 of wave resonance. It might be important for understanding the essential hydrodynamic behavior of the fluid  
87 resonance in the narrow gap.

88 The motivation of this study is to investigate the influence of energy transformation and energy dissipation  
89 on the hydrodynamic behavior of wave responses around the resonant frequency. In the previous studies, all  
90 floating objects were modelled as the identical bodies, whereas in reality the objects may have different sizes,  
91 such as the most typical loading or offloading operations of the side-by-side arrangement between FPSO and  
92 LNG vessels. Therefore, the system with two non-identical boxes is taken as the background of this study, as  
93 the non-identical nature of the system may affect both the resonant frequency and amplitude in the narrow  
94 gap compared to the identical box systems. Besides the wave amplitude in the narrow gap, the reflection and  
95 transmission coefficients are also attributed to the process of energy transformation. Moreover, the quadratic  
96 sum of the reflection and transmission coefficients,  $\mathbb{E} = K_r^2 + K_t^2$ , defined as energy coefficient, is adopted  
97 for examining the energy dissipation. Under the framework of linear potential flow theory, the principle of  
98 energy conservation ensures the energy coefficient keeps at  $\mathbb{E} = 1$ . The value of  $\mathbb{E}$  by the present viscous flow  
99 model can give us a new view on the energy dissipation due to the influence of fluid viscosity. In sum, an  
100 integral comprehensive understanding on the mechanical essence of the gap resonance is expected from the  
101 perspective of energy transformation and energy dissipation in the current study.

102 In Sections 2, 3 and 4, the numerical wave flume used in this work is presented, setup and validated  
103 against available experimental and numerical data, respectively. The numerical results and discussions are  
104 presented in Section 5 to show the effect of energy transformation and energy dissipation on wave responses  
105 around the resonant frequency, including the comparisons of results between the linear potential flow model  
106 and the present CFD model, and the influence of gap configuration and incident wave amplitude. Finally,  
107 conclusions are drawn in Section 6.

## 108 2. Mathematical Formulation

109 The governing equations for the mass and momentum conservations in an Eulerian reference system for  
110 incompressible two-phase flows can be given as,

$$\frac{\partial \rho u_i}{\partial x_i} = 0, \quad (1a)$$

111

$$\frac{\partial \rho u_i}{\partial t} + \frac{\partial \rho u_i u_j}{\partial x_j} = \rho g_i - \frac{\partial p}{\partial x_i} + \mu \frac{\partial}{\partial x_j} \left( \frac{\partial u_i}{\partial x_j} + \frac{\partial u_j}{\partial x_i} \right), \quad (1b)$$

112 where  $u_i$  is the velocity component in the  $i$ th direction, and  $u_i^m$  is the velocity component due to the mesh  
 113 deformation in the ALE frame.  $p$ ,  $\rho$  and  $g_i$  are the pressure, fluid density and gravitational acceleration,  
 114 respectively, and  $\mu$  is the fluid dynamic viscosity.

115 In this study, the Volume of Fluid (VOF) method (Hirt and Nichols, 1981), documented by Berberović  
 116 et al. (2009), is adopted to capture the free surface motion. The fractional function of VOF, defined by  $\varphi$ , in  
 117 a computational cell is defined as,

$$\varphi = \begin{cases} 0, & \text{in air} \\ 0 < \varphi < 1, & \text{on free surface} \\ 1, & \text{in water} \end{cases} \quad (2)$$

118 The VOF function satisfies the following advection equation,

$$\frac{\partial \varphi}{\partial t} + u_i \frac{\partial \varphi}{\partial x_i} = 0. \quad (3)$$

119 Herein, the contour of VOF function with  $\varphi = 0.5$  is used to represent the interface between the water and  
 120 air phases. In the computations, the fluid density and effective viscosity are averaged by using the available  
 121 VOF function,

$$\rho = \varphi \rho_W + (1 - \varphi) \rho_A, \quad (4a)$$

122

$$\mu = \varphi \mu_W + (1 - \varphi) \mu_A, \quad (4b)$$

123 where the subscripts  $W$  and  $A$  represent the Water phase and Air phase, respectively.

124 In the present numerical wave flume, relaxation zones are adopted to generate the incident wave and  
 125 eliminate the transmission wave at the inlet and outlet boundaries, respectively. Moreover, it can also be  
 126 implemented to avoid the internal wave reflection in the computational domain. A relaxation function

$$\alpha_R(\chi_R) = 1 - \frac{\exp(\chi_R^{3.5})}{\exp(1) - 1} \quad \chi_R \in [0, 1] \quad (5)$$

127 is applied inside the relaxation zone in the following way,

$$\vartheta = \alpha_R \vartheta_C + (1 - \alpha_R) \vartheta_T, \quad (6)$$

128 where  $\vartheta$  is either  $u_i$  or  $\varphi$ , and the subscripts  $C$  and  $T$  represent the Computed value and Target value,  
 129 respectively. The variation of  $\alpha_R$  is the same as in Fuhrman et al. (2006), where  $\alpha_R$  in Eq. (5) is only  
 130 activate in the relaxation zone, and it is always 1 at the interface between the non-relaxed part of the  
 131 computational domain. Detailed information about the relaxation technique can be found in Mayer et al.  
 132 (1998), Engsig-Karup (2006) and Jacobsen et al. (2012).

133 The governing equations (1a)-(1b) and the VOF equation (3) are solved based on the Finite Volume  
 134 Method (FVM) integrated in the OpenFOAM<sup>®</sup> package. The velocity and pressure are decoupled by the  
 135 Pressure Implicit with Splitting of Operators algorithm (PISO) (Issa, 1986). The Euler method is used to  
 136 discretize the transient term. The convection term and diffusion term are discretized by the Gauss Limited  
 137 Linear method and the Gauss Linear Corrected method, respectively. The numerical computations always  
 138 start from the still state, which means the hydrostatic pressure and zero velocity are specified as the initial  
 139 conditions. The no-slip boundary condition is imposed at the solid wall including the body surface and  
 140 seabed. At the upper boundary of the numerical wave flume, a reference pressure  $p = 0$  and a velocity  
 141 condition  $\frac{\partial \mathbf{u}}{\partial \mathbf{n}}$  are implemented with  $\mathbf{n}$  the outward unit normal vector. The interface tension between the  
 142 air and water phases is neglected in this study since the dynamic effects from the air phase are very small.  
 143 At the two ends of the spongy layer, zero velocities are applied considering that the waves are damped out  
 144 there by the spongy layer. For the details of numerical implements in OpenFOAM<sup>®</sup>, the readers may refer  
 145 to Jasak (1996) and Rusche (2003).

146 In the present numerical simulation, the time increment is automatically determined according to the  
 147 Courant-Friedrichs-Lewy (CFL) condition,

$$\Delta t \leq C_r \times \min\{\sqrt{S_e}/|u_e|\}, \quad (7)$$

148 where  $S_e$  and  $|u_e|$  are the area and absolute velocity in a computational cell, respectively. The numerical  
 149 experience in the present study confirms that the coefficient  $C_r = 0.2$  can produce stable and accurate results.  
 150 It should be mentioned that the classical linear potential flow model is also adopted in this study for the  
 151 purpose of comparison, for which the theoretical formulation is omitted here, as it is well known in many  
 152 textbooks.

### 153 3. Numerical Setup

154 The definition sketch of the present numerical simulations is illustrated in Fig. 1, in which the origin  
 155 of the coordinate system is located at the still water level and the wave is propagating in the positive  $x$   
 156 direction. Two boxes, defined as Box A and Box B, with the identical breadth  $B = 0.50$  m but different  
 157 drafts  $D_L$  and  $D_R$  for the upstream (left) and downstream (right) boxes, respectively, are fixed in a wave  
 158 flume with the water depth  $h = 0.50$  m. A narrow gap with the breadth  $B_g$  is formed by the two boxes,  
 159 where the extremely large amplitude of fluid resonance can be excited as the incident wave frequency is close  
 160 to the natural frequency of the confined fluid bulk. A number of simulation cases are designed to perform the  
 161 intended investigation by varying the values of gap breadth  $B_g$ , and upstream and downstream box drafts  
 162  $D_L$  and  $D_R$ . The definition of the test cases and the corresponding configurations of box drafts  $D_L$  and  $D_R$   
 163 are tabulated in Tab. 1. Four gap breadths  $B_g = 0.030$  m, 0.050 m, 0.070 m, 0.090 m and three incident wave  
 164 amplitudes  $A_i = 0.008$  m, 0.012 m and 0.016 m are selected, so totally 192 different cases are considered.  
 165 In the following descriptions, the prefix 'Bg' would be adopted for identifying the gap breadth, for example

166 Bg50DL103DR205 means  $B_g = 0.050$  m,  $D_L = 0.103$  m and  $D_R = 0.252$  m. The wave frequency  $\omega$  is chosen  
 167 based on the resonant frequency of fluid in the narrow gap, which is the extension of those used in Saitoh  
 168 et al. (2006), Lu et al. (2010) and Moradi et al. (2016).

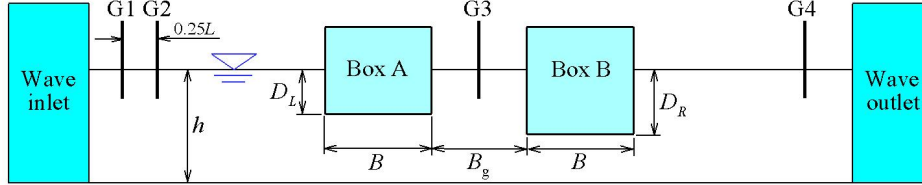


Figure 1: Definition sketch of the numerical wave flume

Table 1: List of test cases and corresponding configurations in the present study

	$D_R = 0.103$ m	$D_R = 0.153$ m	$D_R = 0.202$ m	$D_R = 0.252$ m
$D_L = 0.103$ m	DL103DR103	DL103DR153	DL103DR202	DL103DR252
$D_L = 0.153$ m	DL153DR103	DL153DR153	DL153DR202	DL153DR252
$D_L = 0.202$ m	DL202DR103	DL202DR153	DL202DR202	DL202DR252
$D_L = 0.252$ m	DL252DR103	DL252DR153	DL252DR202	DL252DR252

169 The height of the numerical wave flume is fixed at 0.8 m, and the length is closely relevant to the incident  
 170 wave length  $L$  for different simulations. In numerical simulations, two relaxation zones are arranged on the  
 171 left and right sides of the wave flume, respectively. Generally, the length of the relaxation zone is around  
 172  $1.5 - 2.0L$ . As shown in Fig. 1, four wave gauges, G1-G4, are equipped to record the wave elevation. G1 and  
 173 G2 are used for separating the incident and reflected waves, in which the distance between them is kept at  
 174  $0.25L$ , while G3 and G4 are used to record the wave response in the narrow gap and the transmission wave,  
 175 respectively. G3, G2 and G4 are situated in the middle of the narrow gap,  $1.5L$  from the left side of Box A,  
 176 and  $1.5L$  from the right side of Box B, respectively. In addition, it is noted that we don't restrict  $D_L < D_R$   
 177 in this study.

#### 178 4. Numerical Validation

179 The mesh resolution tests are carried out first by using four different meshes for two kinds of structures,  
 180 Bg30DL103DR103 and Bg70DL252DR252 in Tab. 1. Tab. 2 illustrates the detailed mesh information. Herein,  
 181 non-uniform meshes are adopted for saving the computational time. The square fine meshes with high  
 182 resolution are adopted around the boxes, especially in the vicinity of the narrow gap, to accurately capture  
 183 the large-amplitude free surface oscillation and to account for the boundary layer effect. In the relaxation  
 184 zone of eliminating the transmission wave, coarse rectangular meshes with large aspect ratio up to  $1/20$



185 (height/length) are adopted. As for the relaxation zone of generating the incident wave, square fine meshes  
 186 with intermediate resolution are adopted. Typical meshes in the vicinity of the boxes are shown in Fig. 2,  
 187 which corresponds to Mesh 1 in Tab. 2.

Table 2: Mesh information for convergent tests (Elements/Nodes)

$B_g$ (m)	$D_L = D_R$ (m)	Mesh 1	Mesh 2	Mesh 3	Mesh 4
0.030	0.103	96100/194418	130052/262726	170400/343888	212375/428068
0.070	0.252	100896/204180	131985/266736	162282/327676	221737/447056

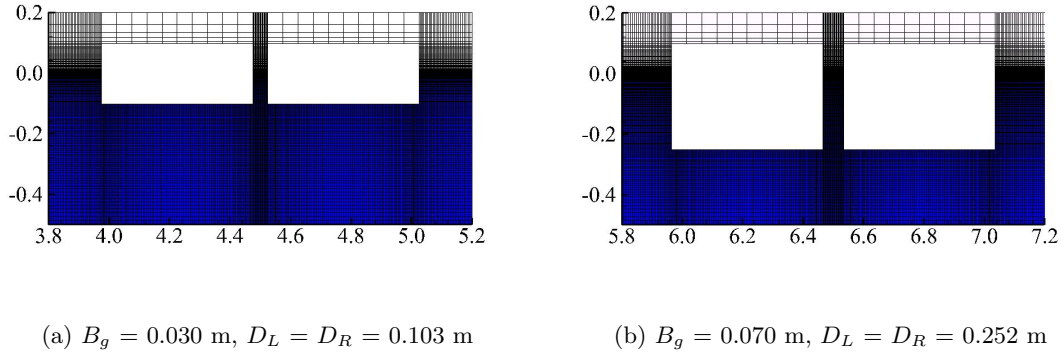
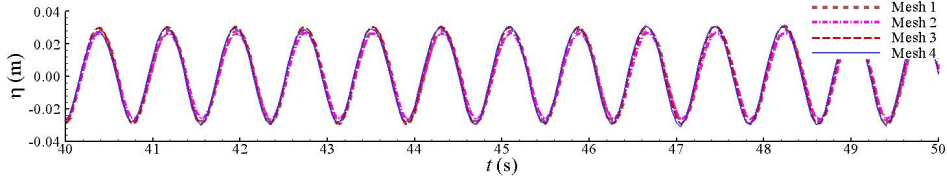


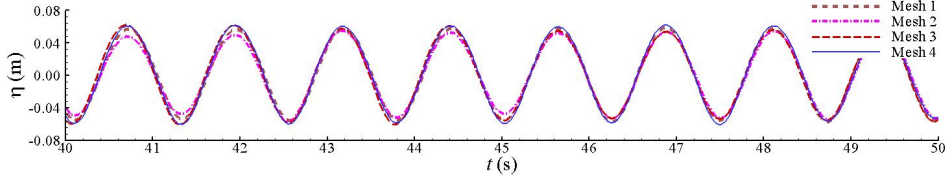
Figure 2: Typical computational meshes in the vicinity of the narrow gap

188 According to the linear potential flow analysis, the resonant frequencies of fluid oscillation in the narrow  
 189 gap can be estimated as 8.00 and 5.10 rad/s for the cases mentioned above, respectively. They are adopted as  
 190 the incident wave frequency for the mesh resolution tests, in which the incident wave amplitude  $A_i = 0.012$   
 191 m is considered. The time signals of wave oscillation in the narrow gap measured at Probe G3 during 40 - 50  
 192 seconds with various mesh resolutions are compared in Fig. 3. A steady state of large-amplitude piston-like  
 193 wave elevations can be observed clearly, implying that the relaxation zones can work well in eliminating the  
 194 reflection and transmission waves. Very little discrepancy between Mesh 3 and Mesh 4 can be observed in  
 195 this figure, which indicate that the convergent solutions can be produced by Mesh 3 for various structures.  
 196 Numerical simulations also suggest that the measured steady-state free surface evolution is quite symmetrical  
 197 and sinusoidal, and the dominating harmonic oscillates at the incident wave frequency  $\omega$  according to the  
 198 Fourier analysis. Furthermore, the normalized wave amplitudes  $A_g/A_i$  in the narrow gap at the Probe G3 are  
 199 compared in Fig. 4. It should be mentioned that the wave amplitudes  $A_g$  in the narrow gap are computed  
 200 by the averaged value of wave amplitudes between the duration of 40 - 60 seconds, after the sensitivity  
 201 analysis by considering different time-windows of 60 - 80 seconds. The comparisons in Fig. 4 suggest that  
 202 the variation of mesh density has little effect on the present numerical results if the number of cells exceeds  
 203  $1.6 \times 10^5$ . Again, Mesh 3 is able to produce convergent solutions, and hence it is adopted as the baseline for

204 the following numerical computations.

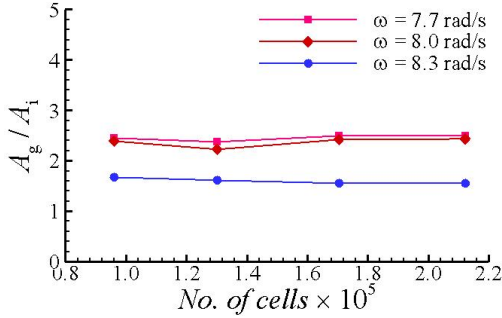


(a)  $B_g = 0.030$  m,  $D_L = D_R = 0.103$  m

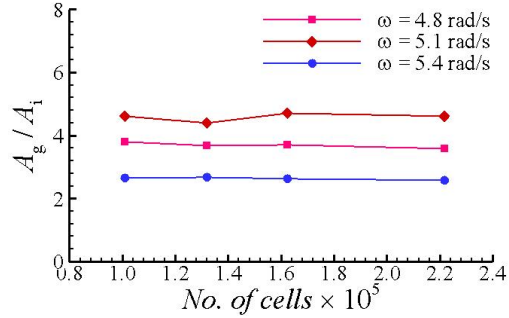


(b)  $B_g = 0.070$  m,  $D_L = D_R = 0.252$  m

Figure 3: Comparisons of wave elevation in the gap under different meshes with various box drafts  $D$  at the resonant frequency  $\omega_g$



(a)  $B_g = 0.030$  m,  $D_L = D_R = 0.103$  m



(b)  $B_g = 0.070$  m,  $D_L = D_R = 0.252$  m

Figure 4: Mesh convergent test for various narrow gap configurations with different incident wave frequencies  $\omega$  around the resonant frequency  $\omega_g$

205 The numerical accuracy of the present numerical model is validated by comparing with the available  
 206 laboratory test results in Saitoh et al. (2006) and the numerical results in Lu, Teng, Cheng, Sun and Chen  
 207 (2011). In their study, only the identical boxes of  $D_L = D_R$  are examined, and hence we denote the drafts  $D_L$   
 208 and  $D_R$  as  $D$  for simplification in this section. The mean normalized wave amplitude  $A_g/A_i$  at G3 (located  
 209 in the center of the narrow gap) is compared in Fig. 5, in which the incident wave amplitude is fixed at  $A_i$   
 210 = 0.012 m and measured by G1 and G2 wave gauges. Again, the averaged wave amplitudes in the steady  
 211 state between 40 - 60 seconds are computed as  $A_g$ . Generally speaking, the present numerical results are  
 212 in agreement with both the experimental measurements and the numerical solutions. All these comparisons

213 confirm that the present numerical wave flume works well in predicting wave responses, including the resonant  
 214 frequency and amplitude in the narrow gap. The relationship between the structure configuration, resonant  
 215 frequency and resonant amplitude can also be observed in Fig. 5. With increasing the gap breadth and box  
 216 draft, the resonant frequency becomes smaller. In addition, the resonant wave amplitude in the narrow gap  
 217 increases with the increase of box draft. All these phenomena are similar to those presented in the previous  
 218 investigations.

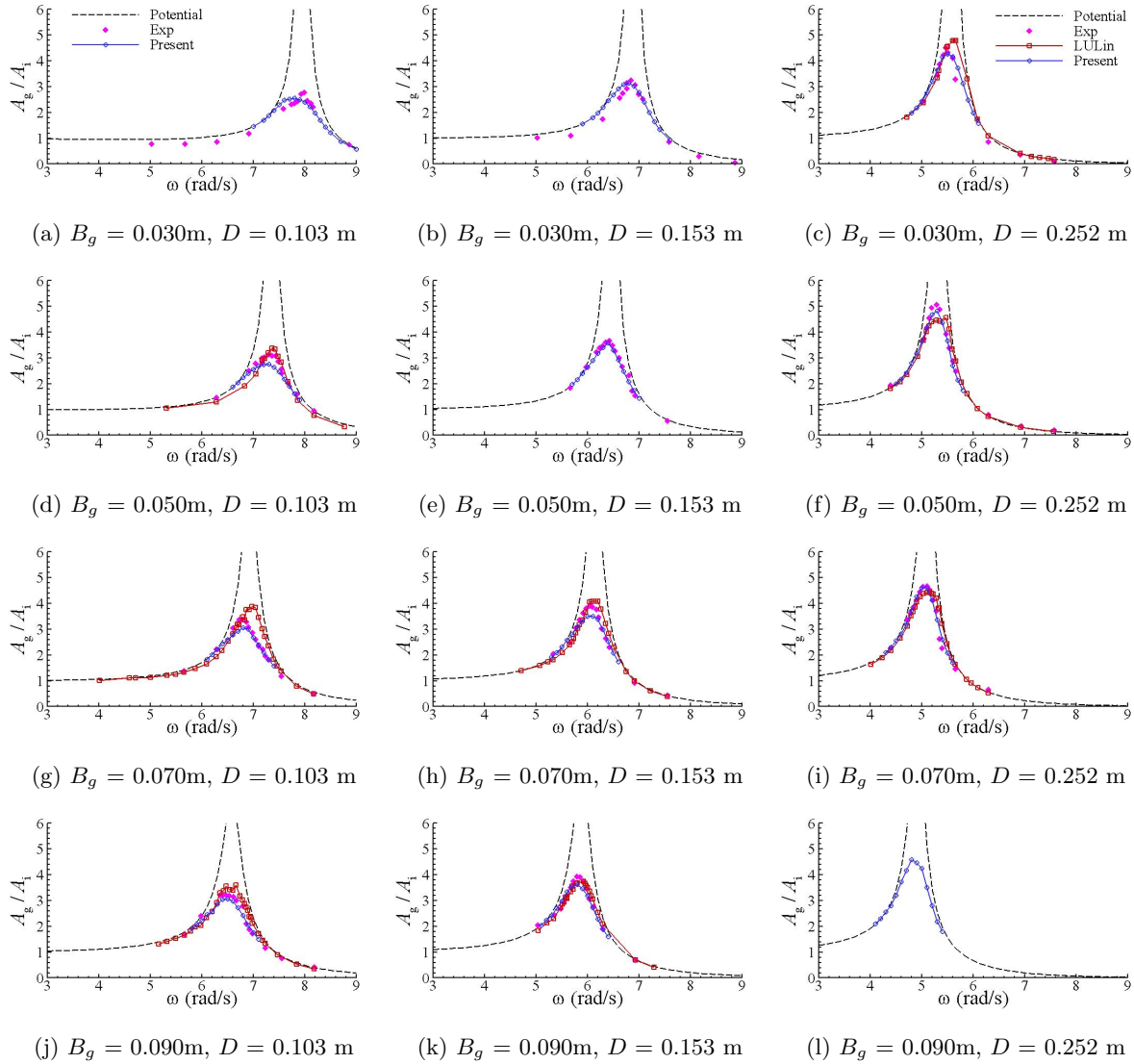


Figure 5: Comparison of normalized wave amplitude  $A_g/A_i$  for various gap breadths and drafts

219 Validations are also extended to the results of reflection and transmission coefficients in this work. The  
 220 reflection and transmission coefficients are defined as  $K_r = A_r/A_i$  and  $K_t = A_t/A_i$ , respectively, where  $A_r$   
 221 and  $A_t$  are the reflected and transmitted wave amplitudes, measured at Probes G1, G2 and G4. In accordance  
 222 with the wave amplitudes in the narrow gap,  $A_r$  and  $A_t$  are also the averaged wave amplitudes in the steady

223 state between 40 - 60 seconds. Fig. 6 depicts the comparisons of reflection and transmission coefficients,  $K_r$   
 224 and  $K_t$ , for Bg50DL252DR252 between the present numerical results, the measured data in Saitoh (2007)  
 225 and the numerical results in Lu et al. (2010). In addition, for the purpose of comparison, results by the  
 226 potential flow model are also presented in this figure. Fig. 6a shows that for the reflection coefficient, the  
 227 frequency of the minimal peak value predicted by the viscous fluid models and potential flow model are  
 228 almost identical to the observation in the experiments, which is the resonant frequency of fluid oscillation in  
 229 the narrow gap. The variations of  $K_r$  against  $\omega$  predicted by the two viscous models are found to be in good  
 230 agreement with the experimental data. Whereas, the potential flow model gives a significant minimal peak  
 231 value at the resonant frequency. The discrepancies between the two sets of viscous fluid numerical results  
 232 at the high wave frequencies might be due to the different numerical models adopted. The numerical model  
 233 adopted in Lu et al. (2010) is the three-step high-order upwind Taylor-Galerkin FEM, where the issue of  
 234 numerical dissipation might need more attention. As the increase of incident wave frequency, the increasing  
 235 wave steepness is expected, leading to more numerical dissipation in the numerical simulations, especially in  
 236 the region of high wave frequency in Fig.6a. As for the predictions of transmission coefficient in Fig. 6b, the  
 237 maximal value of transmission coefficient predicted by the potential flow model is significantly larger than  
 238 that in the experimental tests and by the viscous fluid models.

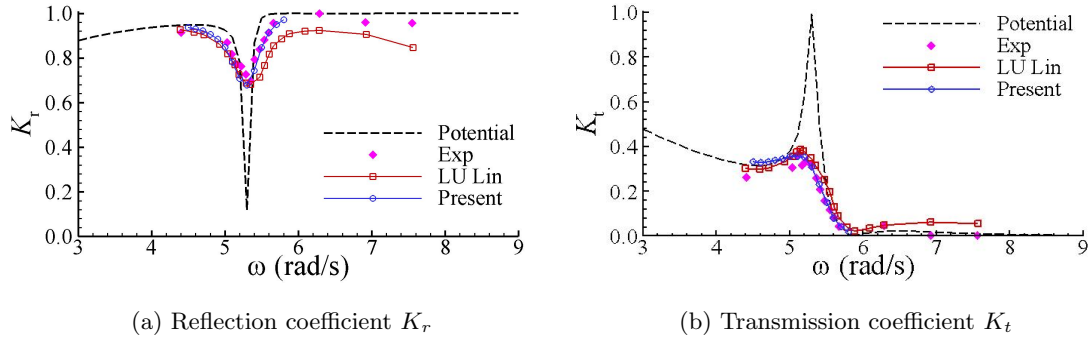


Figure 6: Comparison of reflection and transmission coefficients for the case of  $B_g = 0.005$  m,  $D_L = 0.252$  m and  $D_R = 0.252$  m

239 The comparisons shown in Figs. 5 and 6 confirm that the present numerical wave flume works well, and  
 240 is capable of producing numerical results in good agreement with the experimental data both on the wave  
 241 amplitude in the narrow gap and the reflection and transmission coefficients. However, the potential flow  
 242 model may over-predict the resonant response in the narrow gap and the minimal and maximal values of the  
 243 reflection and transmission coefficients.

## 244 5. Numerical Results and Analysis

245 The validation study in the previous section shows that the present numerical wave flume is able to  
 246 reproduce well the studied scenario of gap resonance between two rectangular boxes. It is employed to

247 investigate the fluid resonance in the narrow gap formed by two non-identical boxes under wave actions.  
 248 As mentioned above, in total 192 cases listed in Tab. 1 are considered herein. In order to demonstrate the  
 249 necessity of adopting the viscous fluid model for this problem, the linear potential flow solutions are also  
 250 included for the purpose of comparison. Numerical results include the resonant wave amplitude in the narrow  
 251 gap, the reflection and transmission coefficients of the two-box system, and the quadratic sum of reflection  
 252 and transmission coefficients,  $\mathbb{E} = K_r^2 + K_t^2$ , defined as energy coefficient for examining the energy dissipation.  
 253 Again, all these parameters are computed by the averaged values in the steady state between 40 - 60 seconds.

### 254 5.1. General description of wave response

255 Numerical investigations begin with the variation of wave response in the narrow gap against the incident  
 256 wave frequency with the incident wave amplitude  $A_i = 0.012$  m, for the cases of  $B_g = 0.050$  m, as shown  
 257 in Fig. 7. It is found that the resonant frequency predicted by the two numerical models is almost identical  
 258 for each gap configuration considered in this work. However, the significant over-predicted resonant wave  
 259 amplitudes in the narrow gap can be observed in the potential flow results. The major reason for the  
 260 over-prediction is that the potential flow theory, in which the fluid is assumed to be inviscid and the flow  
 261 irrotational, cannot model the influence of the fluid viscosity correctly. On the other hand, the potential flow  
 262 model can work well if the incident wave frequencies are outside the range of resonant frequencies. At these  
 263 frequencies away from the resonant frequency, the relatively small wave response in the narrow gap can be  
 264 observed, which corresponds to the small wave amplitude on the gap surface and the slow rotational flow  
 265 in the vicinity of the narrow gap. Therefore, the influence of the eddying motion and energy dissipation is  
 266 negligible.

267 Further examinations on the hydrodynamic behavior of the fluid resonant phenomena are extended to  
 268 the reflection and transmission coefficients,  $K_r$  and  $K_t$ , including the results of potential flow and viscous  
 269 fluid flow models. As shown in Fig. 8, the potential flow model can firstly manifest a general impression of  
 270 the variation of  $K_r$  and  $K_t$  with incident wave frequencies. When the incident wave frequency tends to zero,  
 271  $K_r$  and  $K_t$  approach to 0 and 1, respectively, implying the total transmission happens. Oppositely, the total  
 272 reflection phenomenon can be observed when the incident wave frequency gives rise to infinite, leading to the  
 273 results of  $K_r$  and  $K_t$  to be 1 and 0, respectively. This is a typical behavior of the two-dimensional wave-body  
 274 interaction problem, and the effect of wave length is the main reason, which can be simulated by the potential  
 275 flow model, correctly. However, the potential flow model cannot predict an accurate results of reflection and  
 276 transmission coefficients around resonant frequencies. The comparisons of transmission coefficients in Fig. 8  
 277 suggest that the results of the viscous fluid flow model are always much smaller than those of the potential  
 278 flow model. This is because the transmission coefficients are closely connected to the amplitude of wave  
 279 response in the narrow gap. The fluid oscillation in the narrow gap can be taken as a radiation source for  
 280 the downstream wave, leading to the transmission waves. In difference to the linear potential flow analysis,  
 281 the shear shedding and eddying motion due to the fluid viscosity in the narrow gap can reduce the resonant  
 282 wave amplitude, and consequently lead to the smaller transmission coefficient.

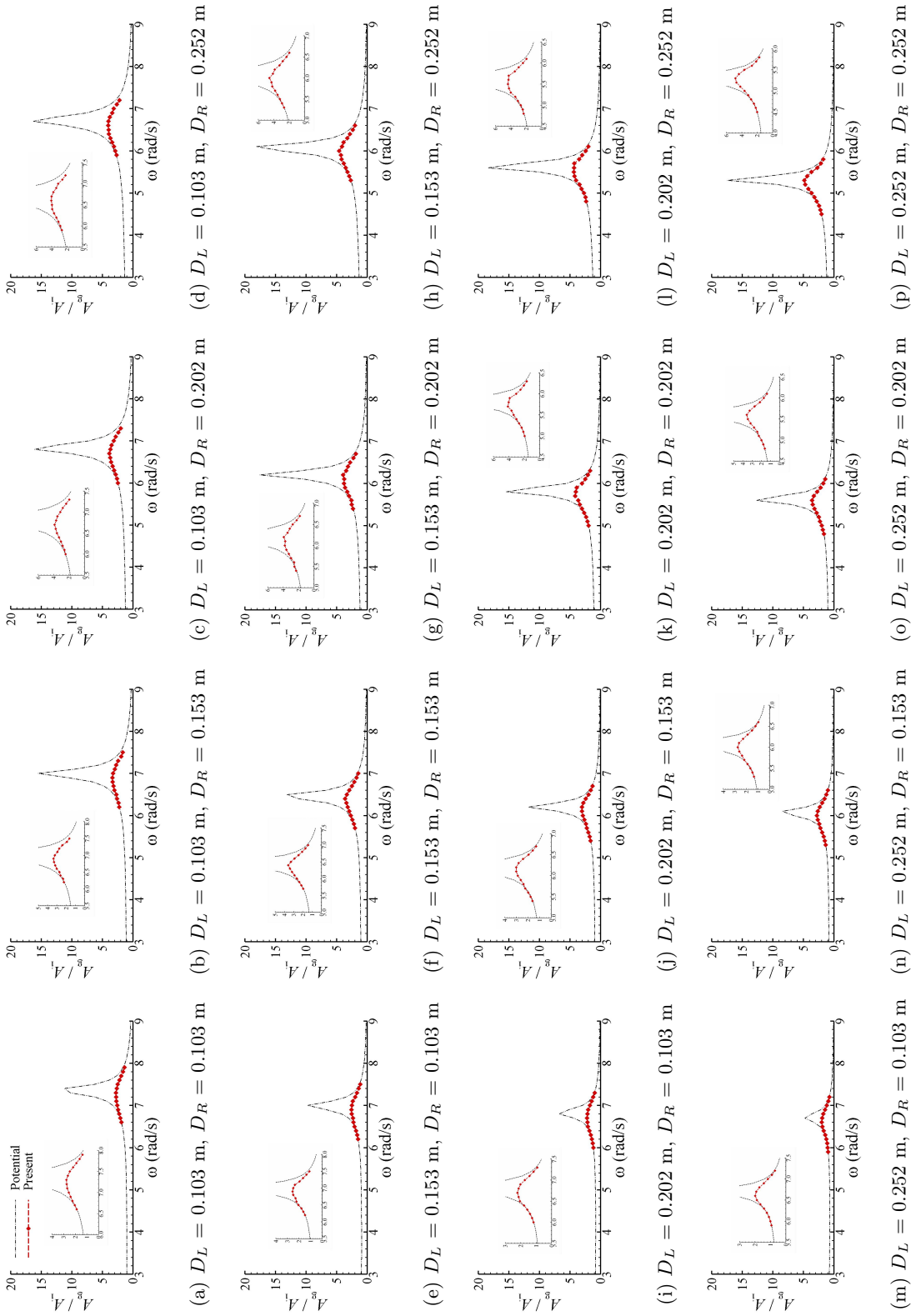


Figure 7: Comparison of normalized wave response  $A_g/A_i$  in the gap for various box drafts

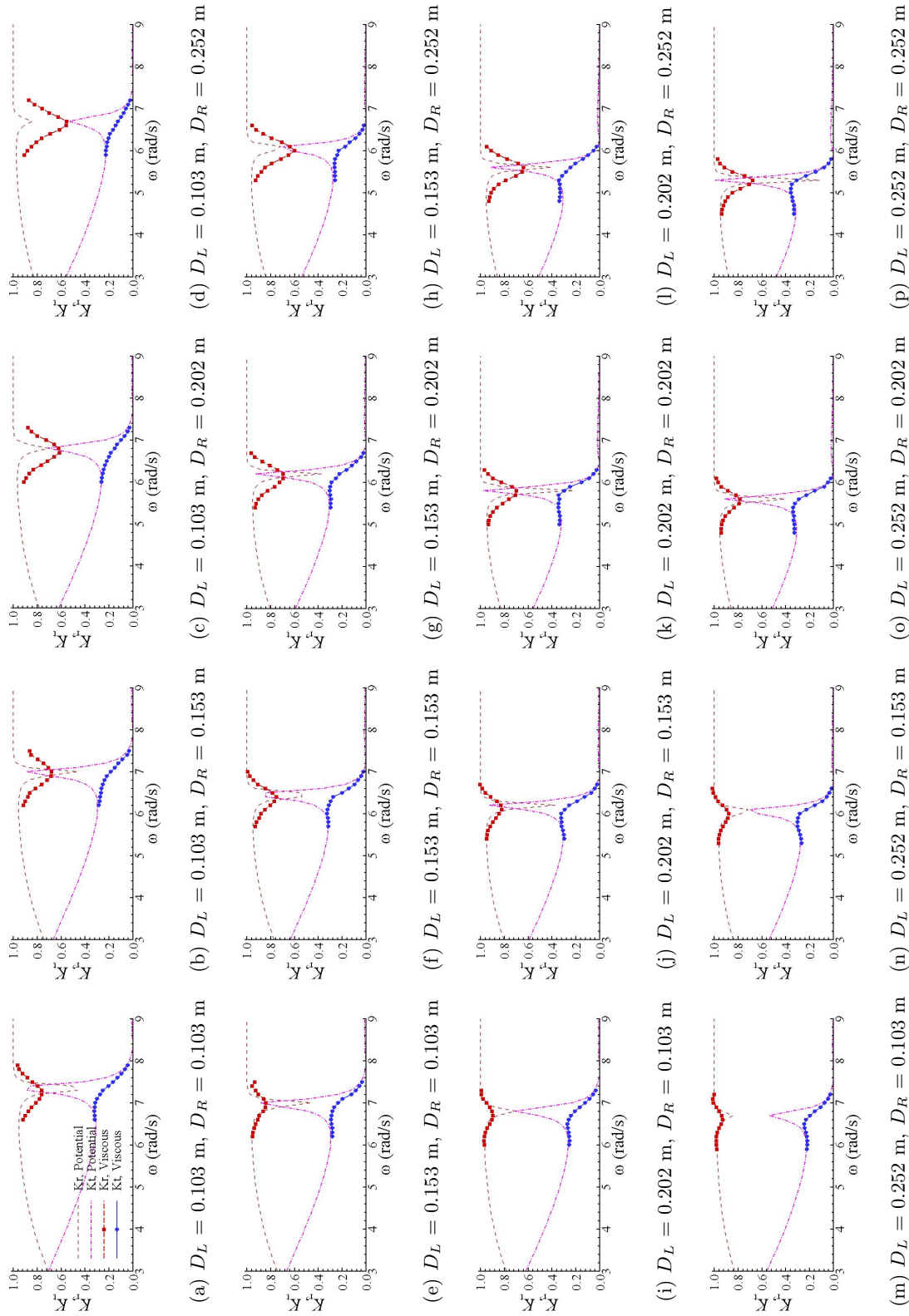


Figure 8: Comparison of reflection and transmission coefficients for various box drafts

283 As for the reflection coefficient, there is no simple regular pattern in the discrepancy between the potential  
 284 flow and viscous flow results. In Figs. 8c, 8d and 8h, the viscous flow results are always smaller than the  
 285 potential flow ones. This is the typical behavior of a system with a smaller upstream and a larger downstream  
 286 box drafts. Because the narrow gap is exposed to the incident wave directly, the large-amplitude piston-mode  
 287 free surface oscillation in the narrow gap can be induced, which can in turn cause the significant energy  
 288 dissipation, leading to the decrease of reflection wave energy. In Figs. 8i, 8m and 8n, the other typical  
 289 behavior of a system with a larger upstream and a smaller downstream box drafts can be observed, in  
 290 which the reflection coefficients by the viscous flow model are always larger than those by the potential flow  
 291 model, and most of the incident wave energy is reflected by the upstream box, leading to the smaller wave  
 292 response and less energy dissipation in the narrow gap. In this case, the energy dissipation in the narrow  
 293 gap between two boxes is not the only dominant issue. The energy transformation due to the reflection  
 294 from the upstream box also play an important role around resonant frequencies. Many factors can affect the  
 295 energy transformation, such as the shielding effect of upstream box on the fluid in the narrow gap, the large-  
 296 amplitude free surface oscillation in front of the two-box system, and so on. In other figures, the reflection  
 297 coefficient given by the viscous flow model are larger than that of the potential flow analysis at the resonant  
 298 frequency for each case. However, the viscous flow results seem to have a wider band, and become smaller  
 299 when slightly away from the resonant frequency, compared to the potential flow results. It is in fact the  
 300 transition between the two typical cases mentioned above. In sum, the reflection coefficient shows different  
 301 hydrodynamic behaviors for various box drafts in Fig. 8, which is closely dependent on the sequence of those  
 302 non-identical boxes.

303 Further analysis is carried out for the quadratic sum of reflection and transmission coefficients,  $\mathbb{E} =$   
 304  $K_r^2 + K_t^2$ , the energy coefficient as defined before. The values of  $\mathbb{E}$  can give us a new view on the energy  
 305 dissipation. Fig. 9 shows the results of energy coefficients by both the potential flow and viscous flow  
 306 models. As expected, in the framework of conventional potential flow theory, the law of energy conservation  
 307 determinates the relationship of  $\mathbb{E} = 1$ , indicating no energy is dissipated. As for the viscous flow model,  
 308 a smaller energy coefficient around the resonant frequency can be seen, confirming that significant energy  
 309 dissipation happens. Typical case of smaller upstream and larger downstream box drafts in Fig. 9d gives the  
 310 largest energy dissipation at the resonant frequency among all the cases in Fig. 9. While the smallest energy  
 311 dissipation at the resonant frequency can be found in Fig. 9m, which is the typical case of larger upstream  
 312 and smaller downstream box drafts. Except for wave frequencies in the vicinity of the resonant frequency,  
 313 the energy coefficient gives rise to  $\mathbb{E} = 1$ , implying that the energy dissipation due to the fluid rotational  
 314 motion is negligible.



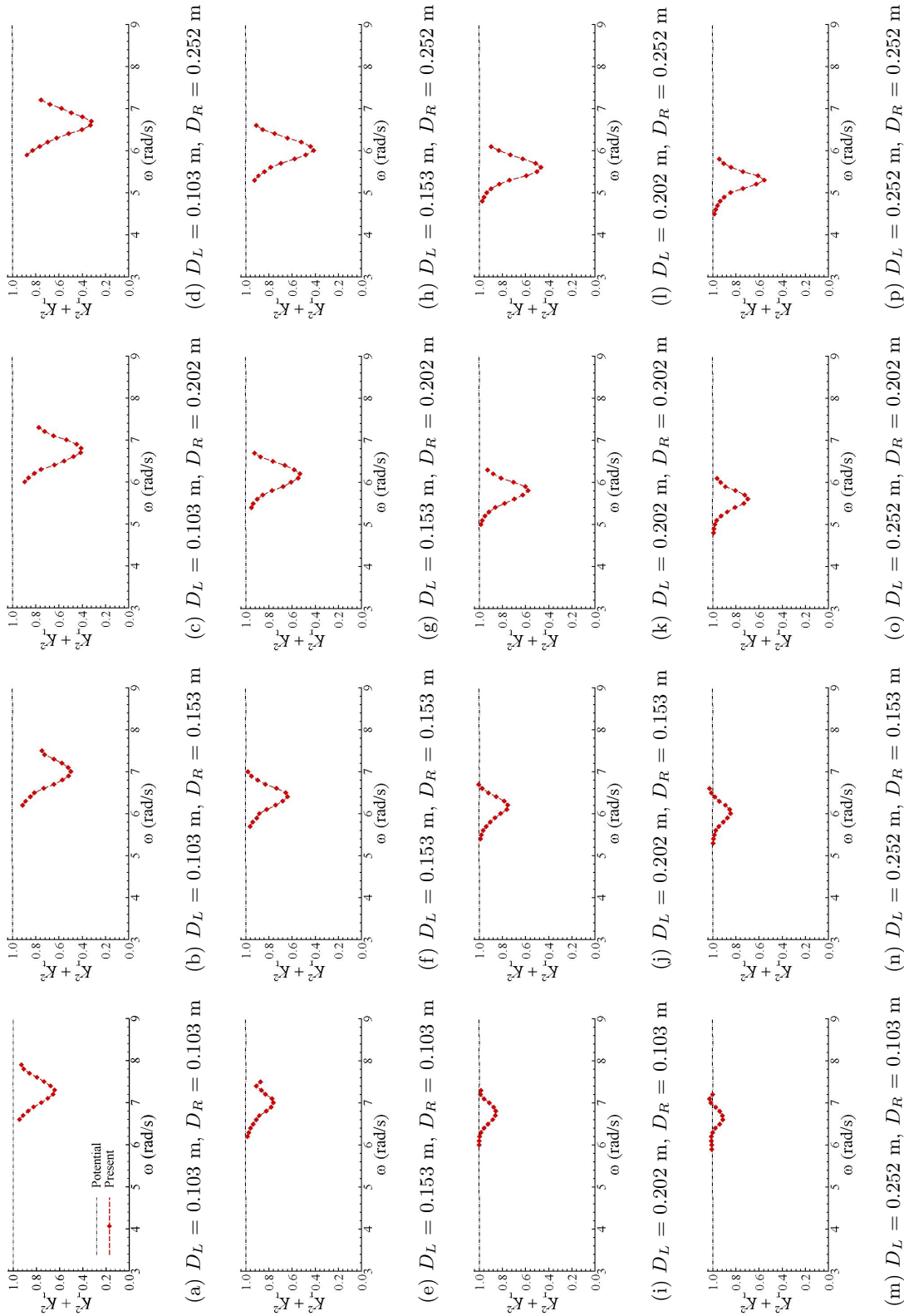


Figure 9: Comparison of energy coefficients for various box drafts

315 *5.2. Influence of downstream box draft*

316 The influence of downstream box draft on the wave response in the narrow gap is investigated in this  
317 section. As shown in Fig. 10, the variation of mean wave amplitude  $A_g/A_i$  in the narrow gap with different  
318 downstream box drafts  $D_R$  is examined. A general comparison suggests that the resonant frequency and  
319 amplitude tend to decrease and increase, respectively, with the increase of downstream box draft. It is believed  
320 that the large-amplitude piston-mode free surface oscillation in the narrow gap is essentially controlled by  
321 the volume of fluid entering into the narrow gap from the gap entrance. The volume of fluid entering into the  
322 narrow gap is dominated by the vertical velocity along the gap bottom. The dependence of wave amplitude in  
323 the narrow gap on the vertical velocity along the gap bottom has been reported in Lu et al. (2010), showing  
324 that the fluid flow in the vicinity of gap bottom has significant effect on wave amplitude in the narrow gap.  
325 Therefore, it is believed that the draft of upstream box is an important factor for the influence of downstream  
326 box draft on the wave amplitude in the narrow gap, which can be demonstrated in Fig. 10. As an example, in  
327 Fig. 10a, the draft of upstream box  $D_L = 0.103$  m is the smallest one. With the increase of downstream box  
328 draft  $D_R$ , the position of gap bottom is kept on 0.103 m. Increasing the downstream box draft  $D_R$  can thus  
329 only enhance the wave action in the vicinity of the gap bottom. As for the case of  $D_L = 0.252$  m in Fig. 10d,  
330 in which the draft of upstream box is the largest one, the position of gap bottom in fact also changes with  
331 the increase of downstream box draft  $D_R$ . This would certainly lead to more sensitive results of the variation  
332 of resonant response for various downstream box drafts in Fig. 10d.

333 Fig. 11 considers the influence of downstream box draft on the reflection and transmission coefficients  
334 around the resonant frequency. It can be seen that the frequency at which the minimal reflection coefficient  
335 occurs decreases with the increase of downstream box draft. Meanwhile, the insignificant variation of trans-  
336 mission coefficient by varying the downstream box draft around the resonant frequency can be observed, cf.  
337 Fig. 11. Correspondingly, the energy coefficient,  $\mathbb{E} = K_r^2 + K_t^2$ , decreases with the increase of downstream box  
338 draft, as shown in Fig. 12. By summarizing the results shown in Figs. 10 - 12, the following process of energy  
339 transformation and dissipation during the fluid resonant oscillation can be suggested. Firstly, the increase  
340 of downstream box draft tends to cause more large-amplitude piston-type of fluid oscillation. More energy  
341 dissipation will happen because the large-amplitude piston-type of fluid oscillation in the narrow gap can  
342 lead to significant fluid rotational motion. Moreover, the increase of fluid oscillation and energy dissipation  
343 is mainly dependent on the energy from the upstream box of the two-box system. It physically expresses the  
344 decrease of reflection coefficient with the increase of downstream box draft. As for the transmission wave,  
345 the downstream box draft has little effect in the present numerical results.

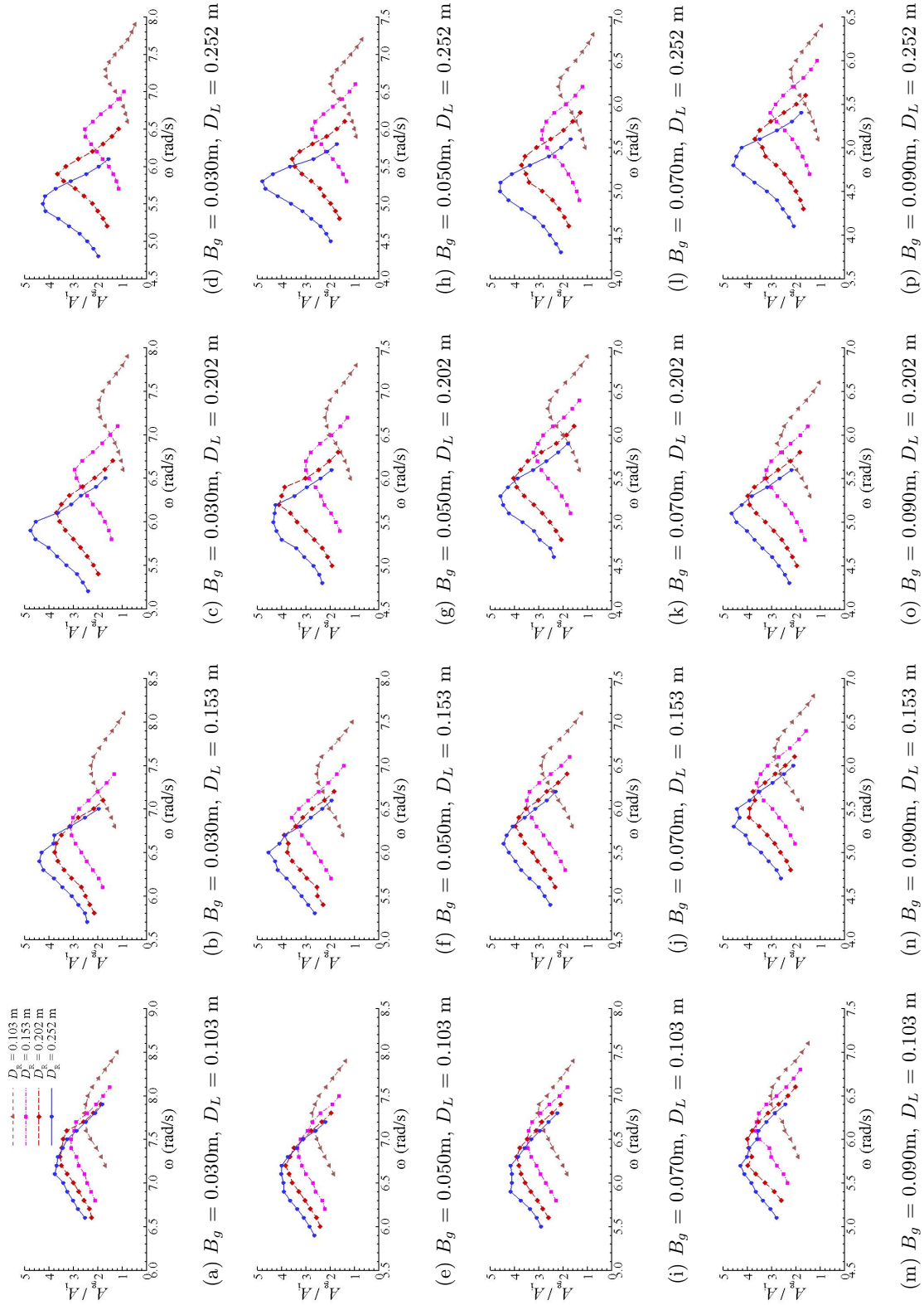


Figure 10: Comparison of normalized wave amplitude  $A_g/A_i$  in the gap for various right box drafts

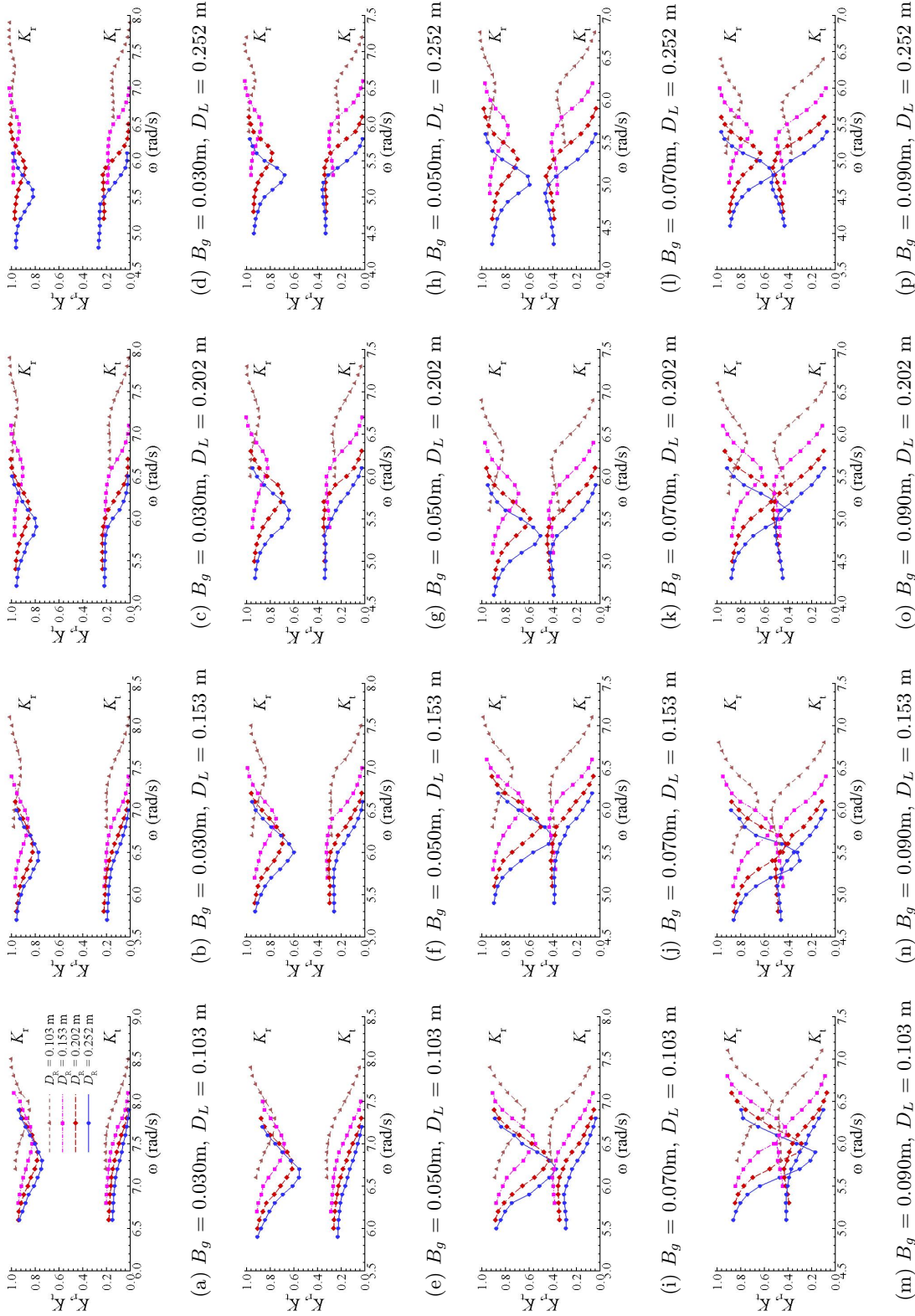


Figure 11: Comparison of reflection and transmission coefficients for various right box drafts

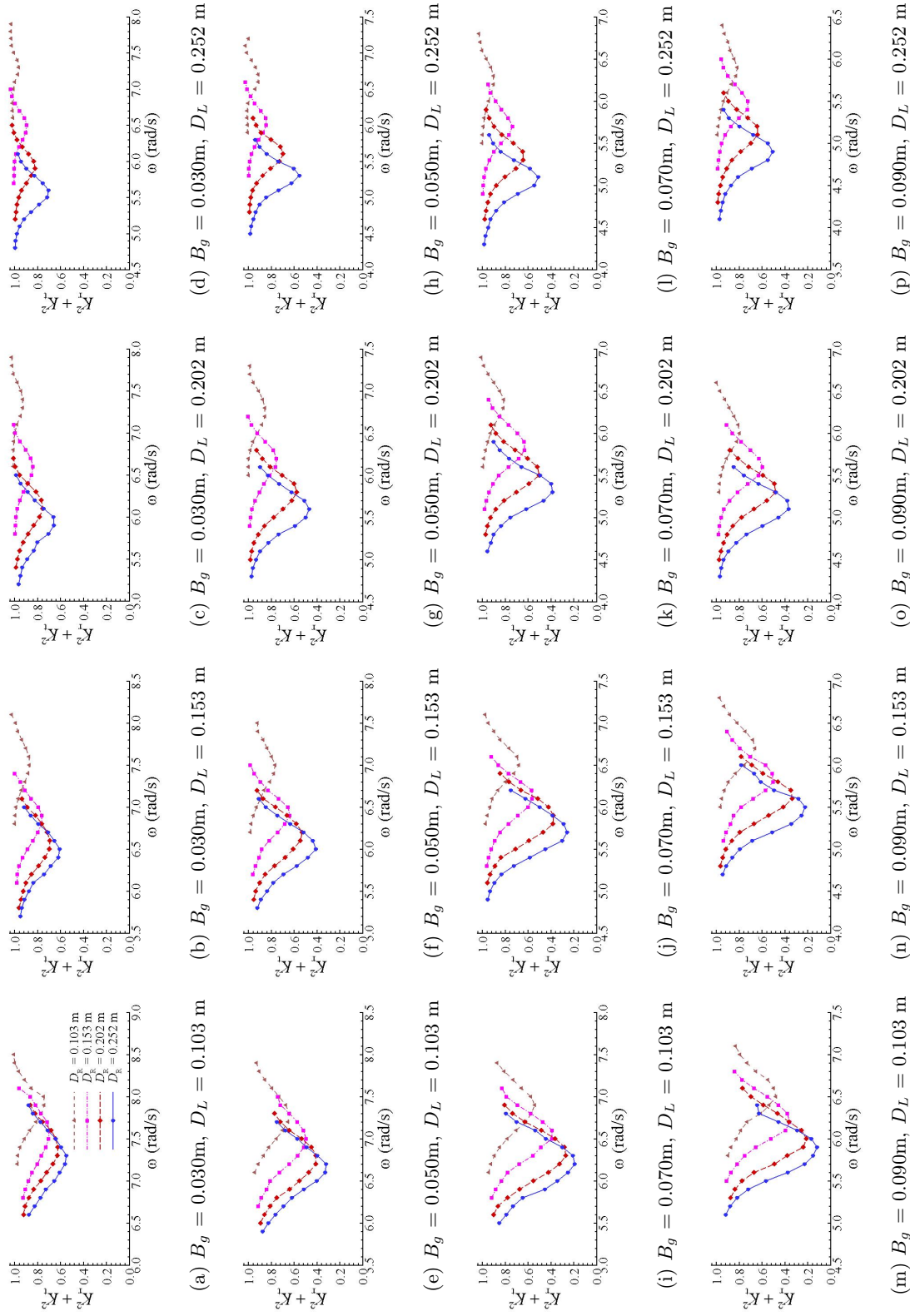


Figure 12: Comparison of energy coefficients for various right box drafts

346 *5.3. Influence of upstream box draft*

347 Fig. 13 shows the influence of upstream box draft on the wave response in the narrow gap. A simple  
348 relation can be observed that the resonant frequency decreases with the increase of upstream box draft.  
349 Variation of resonant amplitude with different upstream box drafts is quite complex in these figures. When  
350 the draft of downstream box is smaller than that of upstream box, the gap bottom is shielded by the upstream  
351 box. It can be understood that the larger  $D_L$  can lead to a stronger shielding effect on this occasion. Typical  
352 examples can be found in the first column of Fig. 13, where the draft of downstream box is the smallest one,  
353  $D_R = 0.103$  m. In this situation, all the resonant amplitudes are observed to be smallest compared to those  
354 with the larger downstream box draft. When the draft of downstream box is larger than that of upstream box,  
355 the gap bottom is exposed to the incident wave action. In this case, the complex hydrodynamic behavior in  
356 the vicinity of the narrow gap is aroused due to the large-amplitude piston-type of resonant fluid oscillation,  
357 including the wave reflection from the leading wall of downstream box, the wave transformation below the  
358 bottom of downstream box, and the vortex shedding from the trailing sharp edge of upstream box. All these  
359 phenomena are not only relevant to the upstream box draft, but also closely dependent on the downstream  
360 box draft and gap breadth. Typical comparisons can be observed in the fourth column of Fig. 13. As for  
361 the second and third columns of Fig. 13, combining the shielding effect and the direct wave action discussed  
362 above, more complex variation of resonant amplitude with different upstream box drafts can be observed.

363 The influence of upstream box draft on the reflection and transmission coefficients is illustrated in Fig. 14.  
364 The increase of upstream box draft can increase the reflection coefficients around the resonant frequency. In  
365 this case, more wave energy is reflected before entering into the two-box system. As for the transmission  
366 coefficient, again, the variation is insignificant compared to the reflection coefficient. In Fig. 15 the increase  
367 of energy coefficient with the increase of upstream box draft can be observed. Finally, comparison between  
368 Fig. 13 and Fig. 15 can also indicate that the large wave oscillations in the narrow gap do not always lead to  
369 the large energy dissipation, such as at the second, third and fourth columns in these figures. The reflection  
370 energy, expressed by the reflection coefficient, is also a significant parameter in this problem.

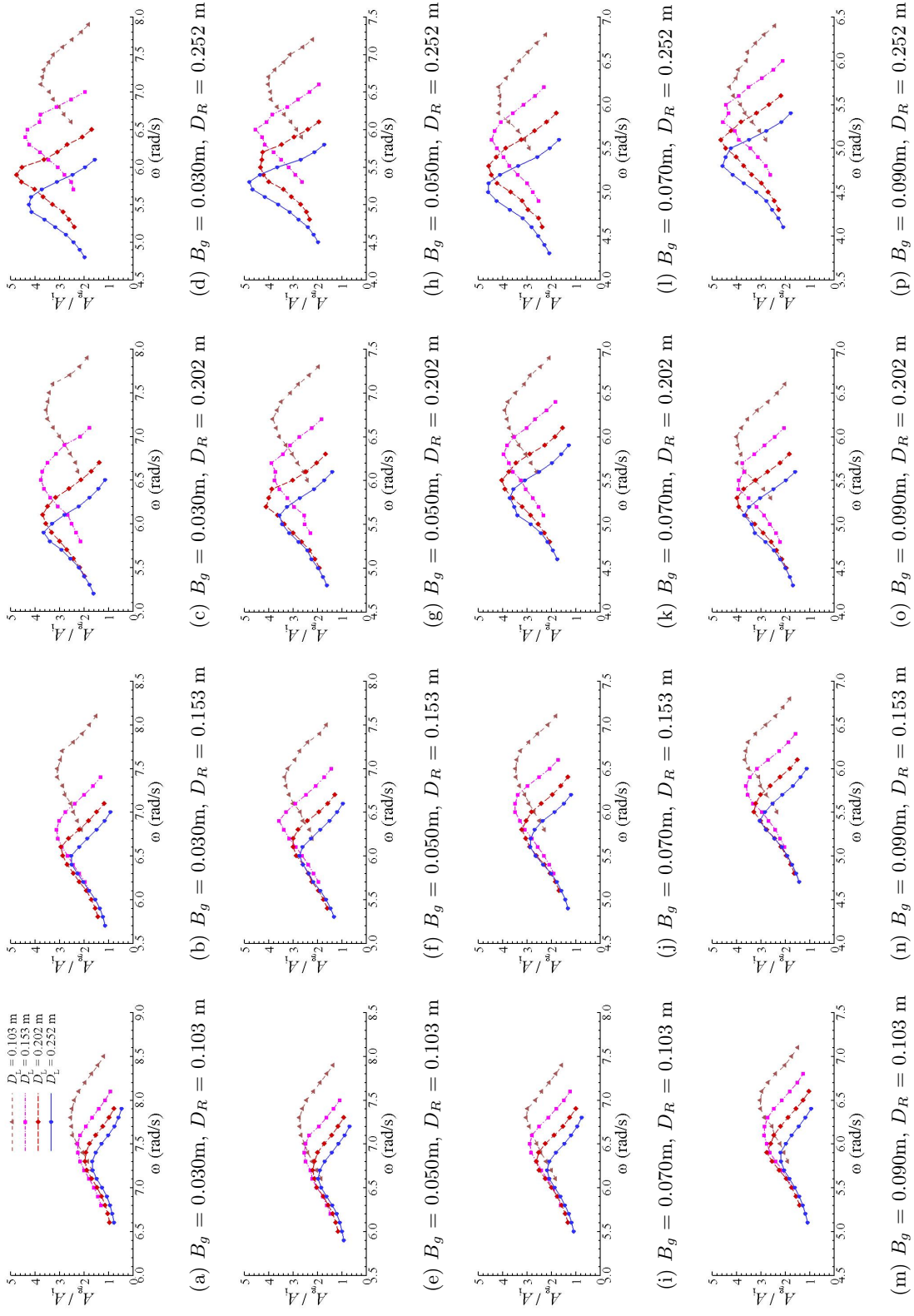


Figure 13: Comparison of normalized wave amplitude  $A_g/A_i$  in the gap for various left box drafts

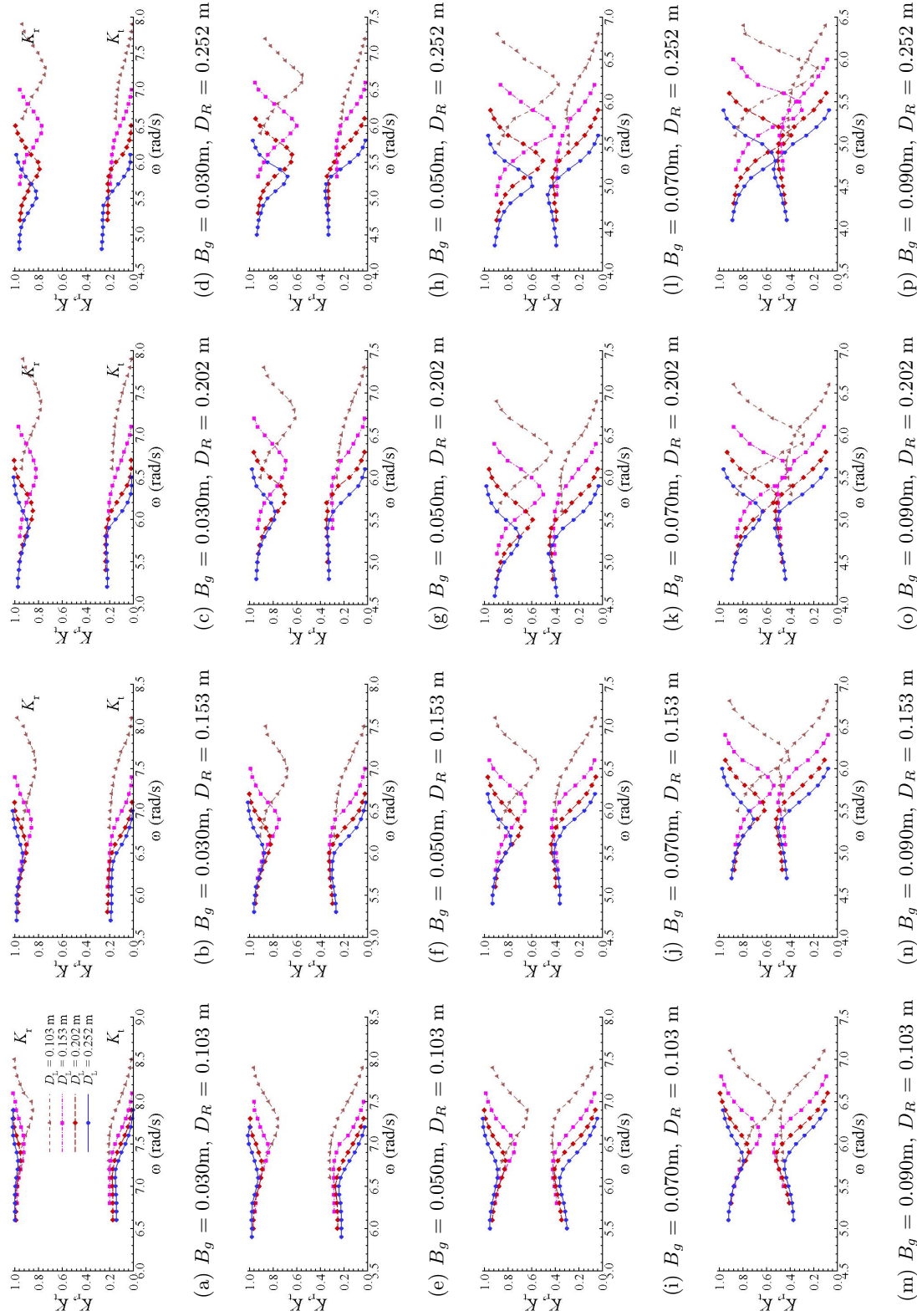


Figure 14: Comparison of reflection and transmission coefficients for various left box drafts



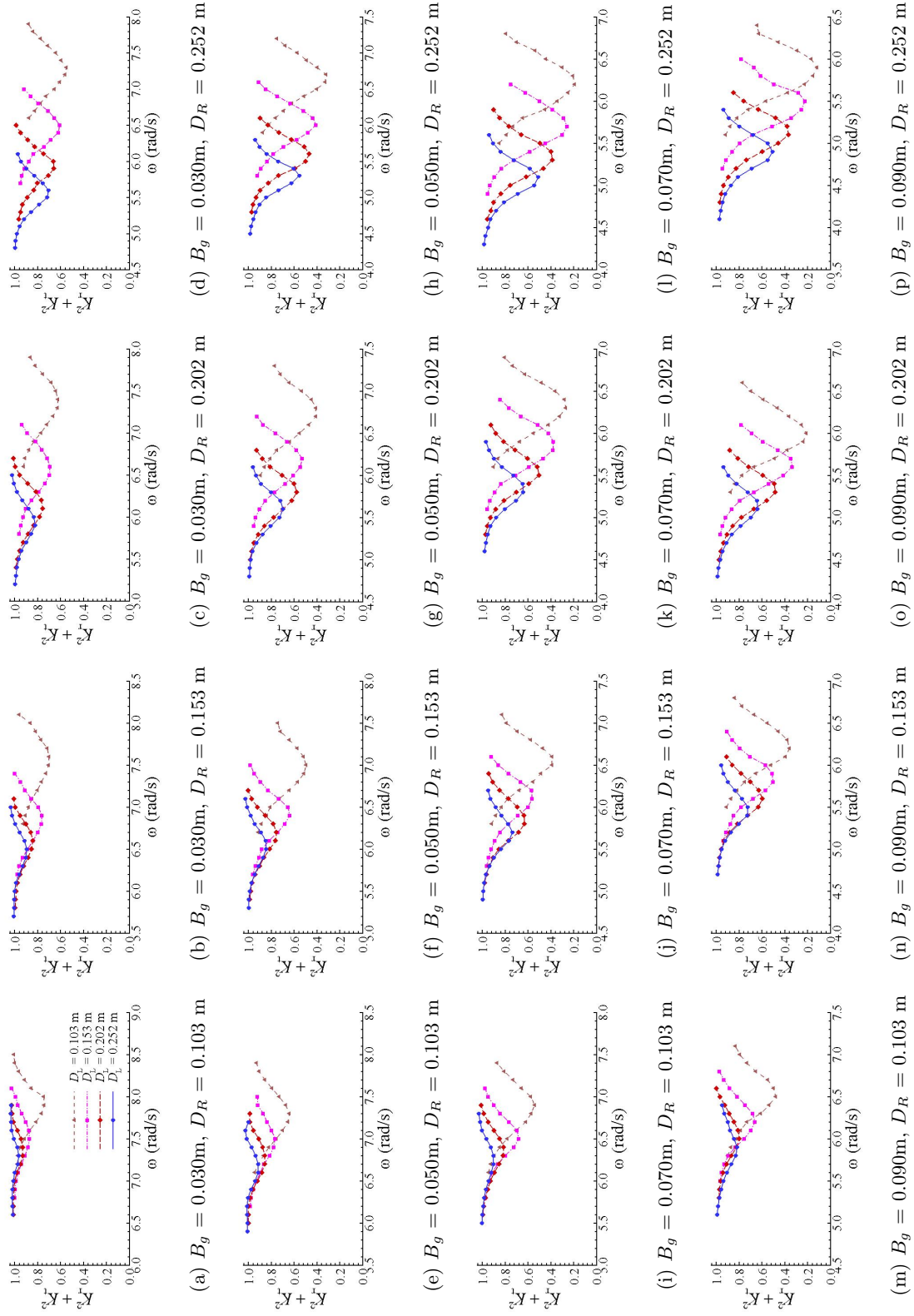


Figure 15: Comparison of energy coefficients for various left box drafts

371 *5.4. Influence of gap breadth*

372 In order to clearly demonstrate the influence of gap breadth on the behavior of wave response in the  
373 narrow gap, the numerical results shown above are re-arranged in Fig. 16. It can be seen from these figures  
374 that for the specific drafts, larger gap breadth can cause smaller resonant frequency. As for the resonant wave  
375 amplitude in the narrow gap, it shows different characters with respect to the gap breadth with different  
376 upstream and downstream box drafts. That is, the effect of gap breadth is dependent on these two parameters.  
377 At the first column of Fig. 16, a general trend of the increase of resonant amplitude with the increase of  
378 gap breadth can be observed. Whereas, at the last column of Fig. 16, it seems hard to found a simple  
379 rule between the resonant amplitude and gap breadth. These phenomena are closely relevant to the wave  
380 reflection, transmission, and fluid rotational motion in the vicinity of the narrow gap.

381 The influence of gap breadth on reflection and transmission coefficients is considered, together with the  
382 energy coefficient. It can be seen from Fig. 17 that the reflection and transmission coefficients decrease and  
383 increase with the increase of gap breadth around the resonant frequency, respectively. Further analysis is  
384 carried out for the energy coefficient in Fig. 18, in which the energy coefficient decreases with the increase  
385 of gap breadth around the resonant frequency. According to the results shown in Figs. 16 - 18, it can be  
386 seen that with the increase of gap breadth, more fluid can be excited to be resonant in the narrow gap, and  
387 more energy is required to support the motion of this bulk fluid. On one hand, this energy comes from the  
388 incident wave, leading to the decrease of reflection coefficient. On the other hand, as a larger radiation source  
389 the oscillation of more fluid can cause the increase of transmission coefficient. It should be noted that more  
390 energy is dissipated due to the more fluid oscillation in the narrow gap. All these phenomena can also result  
391 in the complex hydrodynamic behavior of resonant wave amplitude with the variation of gap breadth.

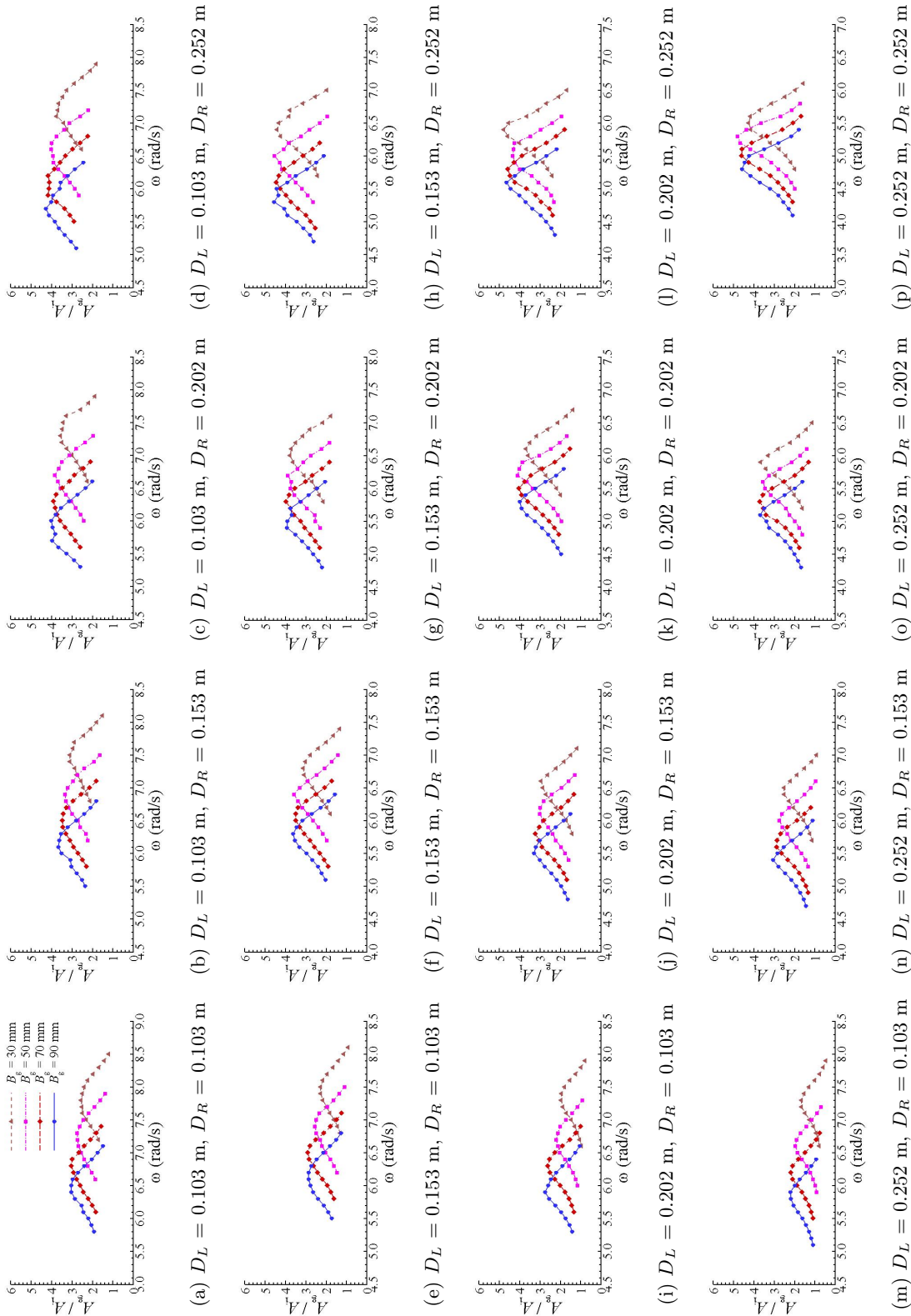


Figure 16: Comparison of normalized wave amplitude  $A_g/A_i$  in the gap for various gap breadths

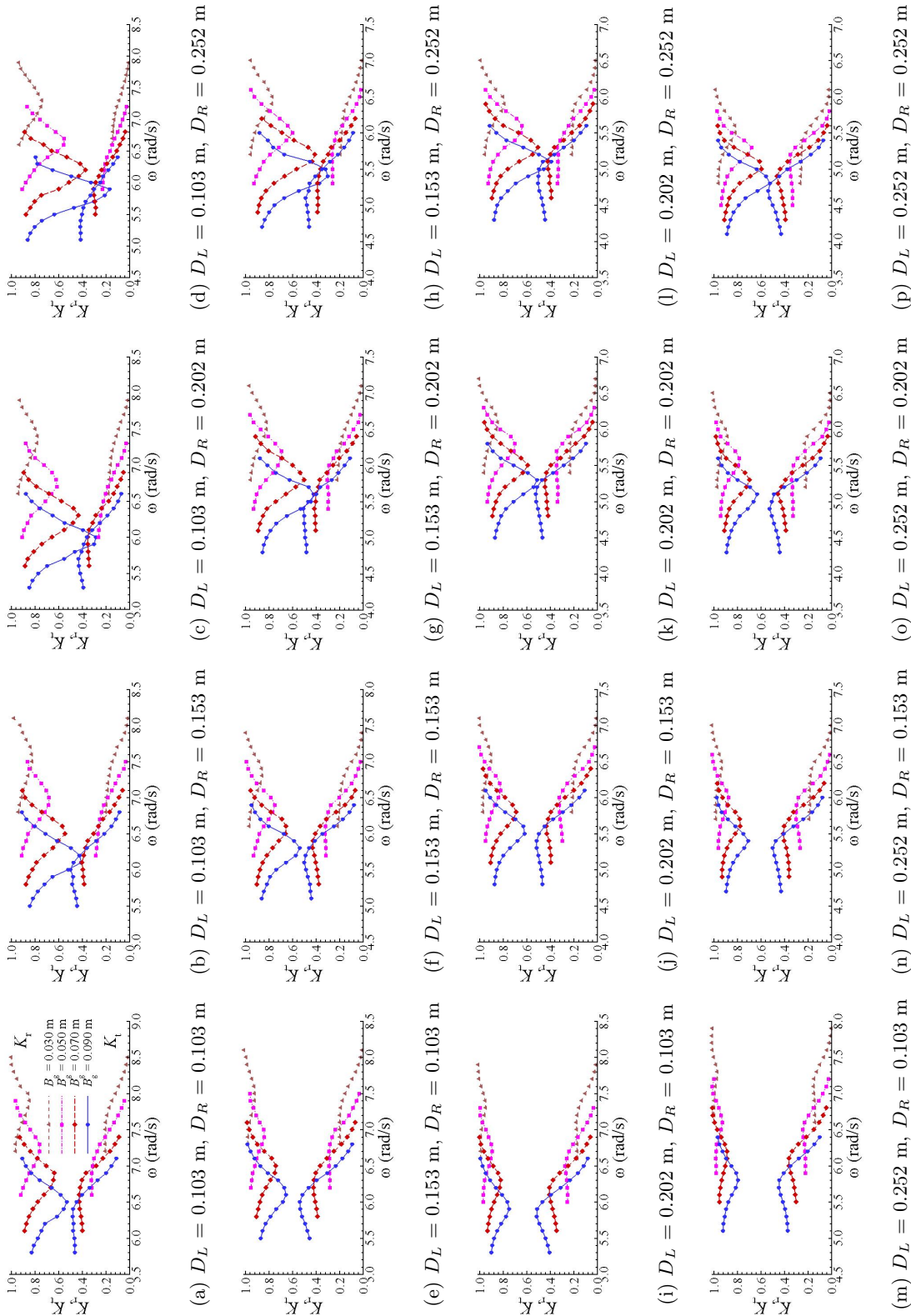


Figure 17: Comparison of reflection and transmission coefficients for various gap breadths

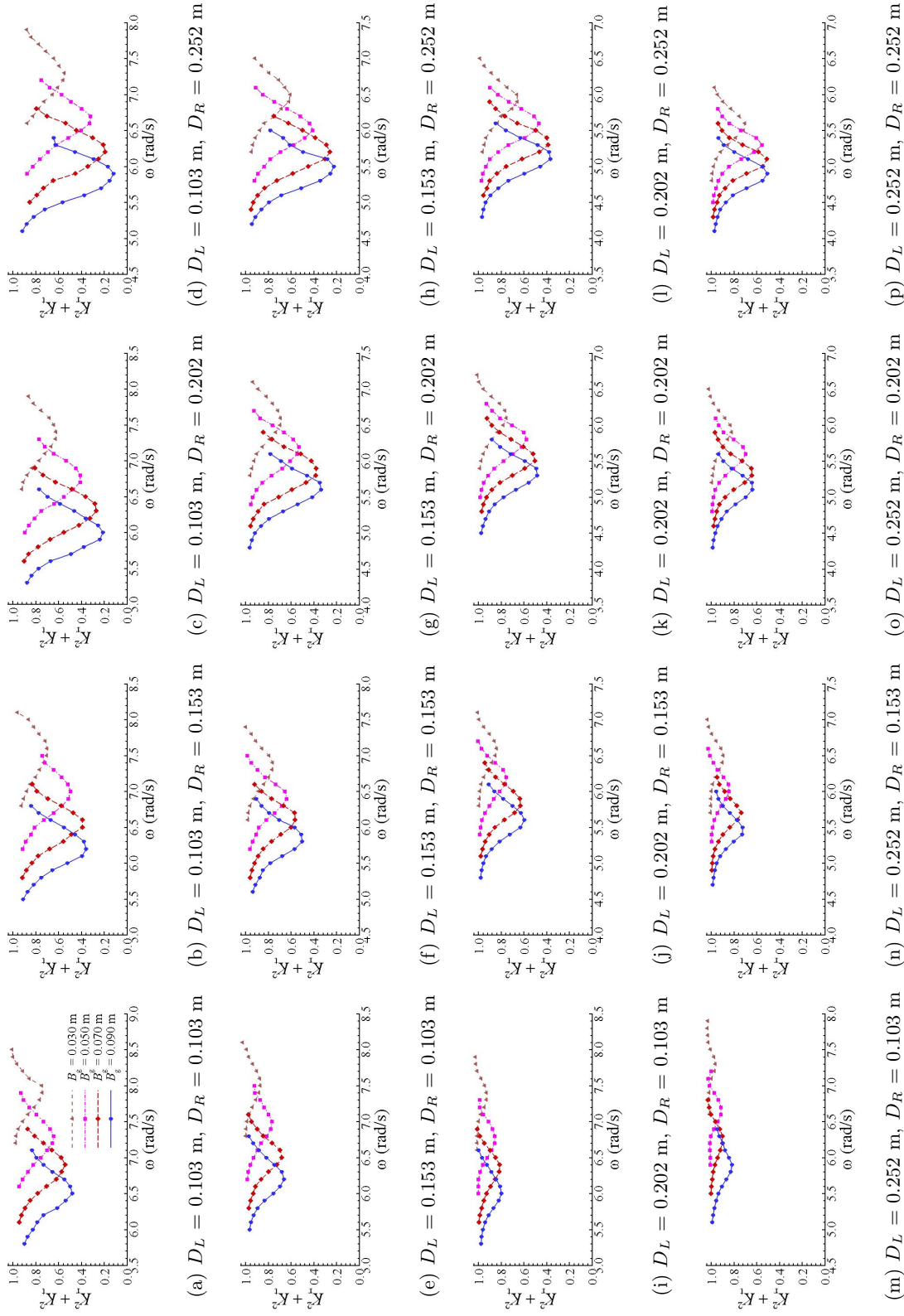


Figure 18: Comparison of energy coefficients for various gap breadths

### 392 5.5. Influence of incident wave amplitude

393 Effect of incident wave amplitude on the wave response in the narrow gap is investigated in this section.  
394 Numerical results of  $B_g = 0.050$  m with various box drafts at three different incident wave amplitudes,  $A_i =$   
395  $0.008$  m,  $0.012$  m and  $0.016$  m, are shown in Fig. 19. It can be seen that for a specific gap parameter, the wave  
396 response in the narrow gap decreases significantly with the increase of incident wave amplitude around the  
397 resonant frequency. However, if the incident wave frequency is far from the resonant frequency, little influence  
398 of incident wave amplitude on the wave response in the narrow gap can be observed. Numerical simulations  
399 also show a slight decrease in the resonant frequency with the increase of incident wave amplitude in Fig. 19.  
400 More detailed comparisons illustrate that the large-amplitude piston-type of free surface oscillation and  
401 significant energy dissipation are relevant to the decrease of resonant frequency. For example, the frequency  
402 corresponding to the maximum amplitude is decreased from  $\omega_g = 6.6$  to  $6.5$  rad/s for Bg50DL103DR252 in  
403 Fig. 19d as the incident wave amplitude increases from  $A_i = 0.008$  m to  $0.016$  m; while it keeps at  $6.6$  rad/s for  
404 Bg50DL252DR103 with those three incident wave amplitudes in Fig. 19m. The increase of mean water level  
405 in the narrow gap due to the free surface nonlinearity, the increase of added mass depending on the response  
406 wave amplitude, and larger damping ratio due to the energy dissipation are the three possible reasons for  
407 the decrease in the resonant frequency. The recent study in Faltinsen and Timokha (2015) quantified a  
408 pressure discharge condition in the gap opening, where a nonlinear integral term was derived in the dynamic  
409 condition on gap surface. It may be fit for further describing the slight decrease of resonant frequency, as  
410 well as measuring the energy dissipation in the vicinity of the gap.

411 The influence of incident wave amplitude on the behavior of reflection and transmission coefficients,  $K_r$ ,  
412 and  $K_t$ , is considered in Fig. 20. Numerical results suggest that the transmission coefficients decrease with  
413 the increase of incident wave amplitude at the resonant frequency, implying that less percent of energy is  
414 transmitted to the downward of the two-body system. On the other hand, the reflection coefficients increase  
415 with the increase of incident wave amplitude at the resonant frequency. Generally, the sensitivity of reflection  
416 coefficient to the variation of incident wave amplitude is stronger than that of transmission coefficient. It in  
417 fact leads to the results in Fig. 21, in which the energy coefficient increases with the increase of incident wave  
418 amplitude at the resonant frequency. In other words, relatively less energy dissipation happens for the large  
419 incident wave amplitude at the resonant frequency. All these phenomena indicate that the increase of incident  
420 wave amplitude with the larger wave amplitude tends to enlarge the reflection energy, and hence relatively  
421 less wave energy can enter into the narrow gap. Therefore, smaller resonant wave response in the narrow  
422 gap and less energy dissipation can be found at the resonant frequency. The analysis demonstrates that the  
423 energy transformation due to the wave reflection is one determinative factor for the decrease of resonant  
424 wave response with the increase of incident wave amplitude at the resonant frequency. Closer comparisons  
425 in Figs. 20 and 21 indicate that the smaller reflection and energy coefficients can be obtained with the larger  
426 incident wave amplitudes at a frequency slightly away from the resonant one, which implies that the relative  
427 energy dissipation due to the fluid rotational motion becomes the dominant factor in this situation. In sum,

428 both the energy transformation and the energy dissipation play the important, but different roles for fluid  
429 resonances in the narrow gap.

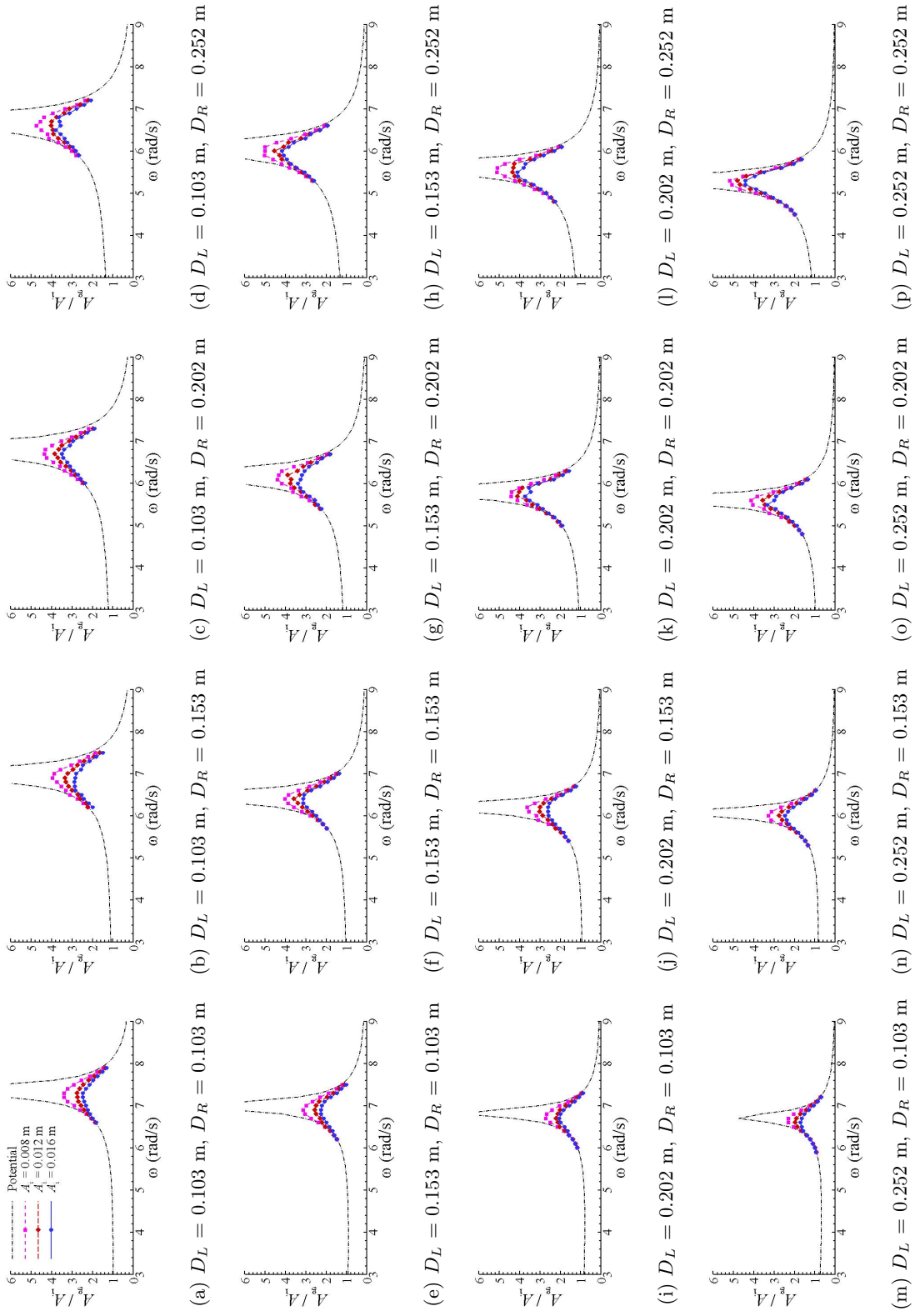


Figure 19: Comparison of normalized wave amplitude  $A_g/A_i$  in the gap for various incident wave amplitudes



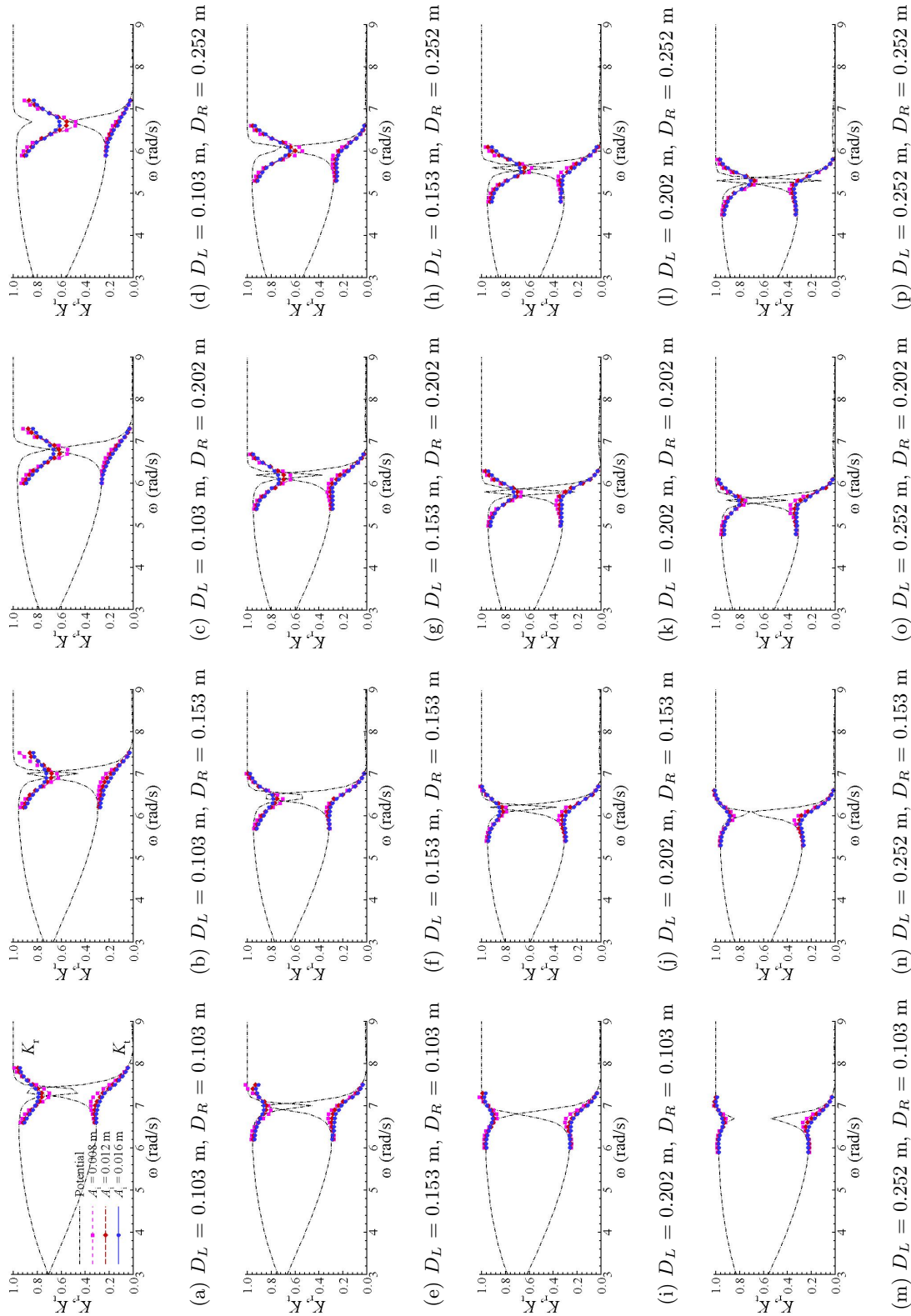


Figure 20: Comparison of reflection and transmission coefficients for various incident wave amplitudes

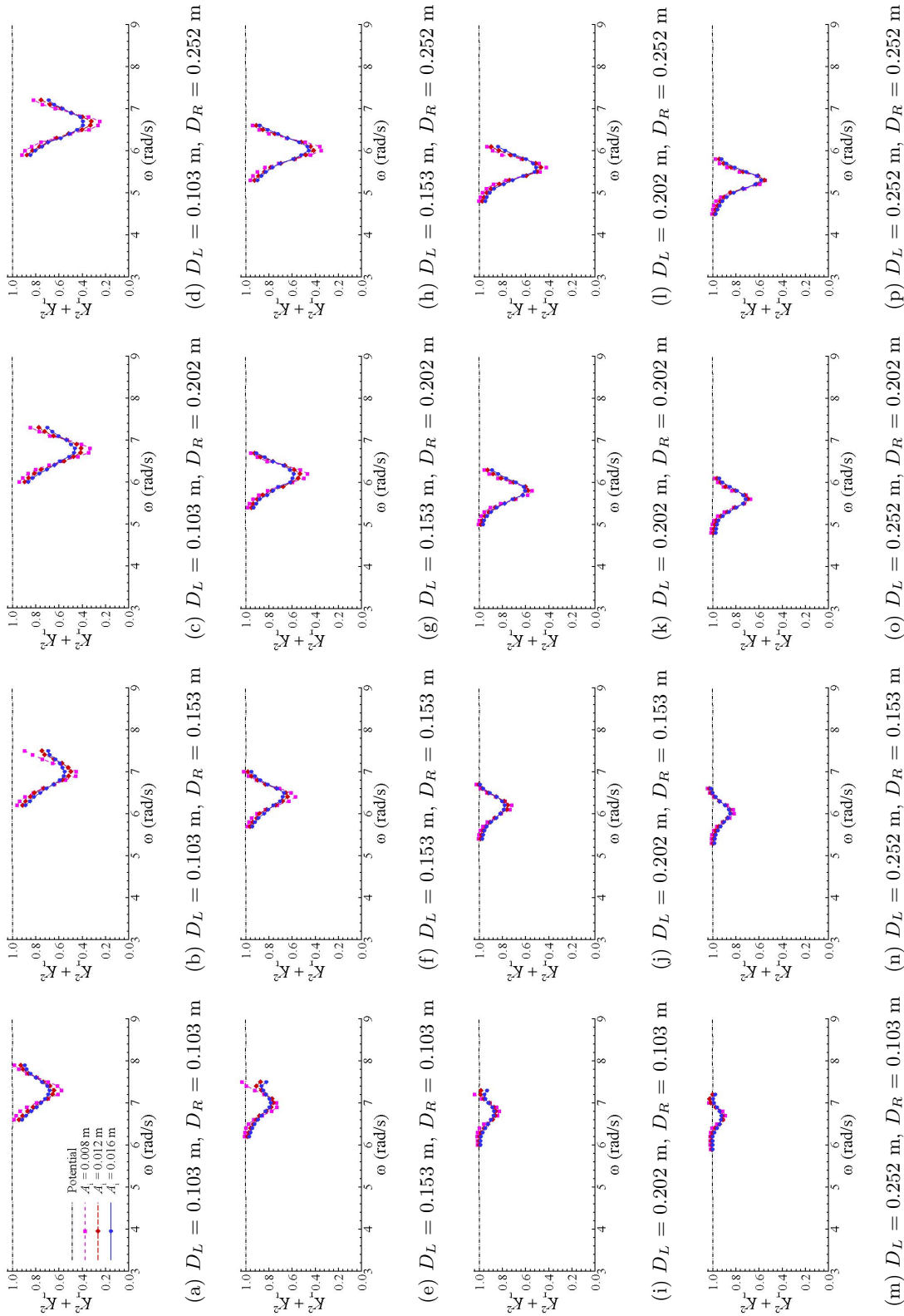


Figure 21: Comparison of energy coefficients for various incident wave amplitudes

## 430 6. Conclusion

431 The Navier-Stokes equations are adopted for investigating the hydrodynamic behaviours of fluid resonance  
432 in the narrow gap formed by two side-by-side non-identical boxes. In order to obtain a clear understanding  
433 of the influence of gap configurations and wave conditions on the wave response, three different incident wave  
434 amplitudes with different frequencies are considered at different gap breadths, upstream and downstream  
435 box drafts, comprising in total 192 different cases. Numerical investigations include the wave amplitude in  
436 the narrow gap, the reflection and transmission coefficients,  $K_r$  and  $K_t$ , and the energy coefficient, defined  
437 as  $\mathbb{E} = K_r^2 + K_t^2$ . The mechanical essence of the gap resonance between two non-identical boxes is explained  
438 from the perspective of energy transformation and energy dissipation. The main findings are illustrated as  
439 follows:

- 440 1) Consistent with the theoretical analysis, the numerical simulations suggest that the resonant frequency  
441 tends to be smaller with the increase of gap breadth, upstream and downstream box drafts. The incident  
442 wave steepness hardly affects the resonant frequency; only a slight decrease of the resonant frequency can  
443 be observed with the increase of incident wave amplitude for the cases with larger energy dissipation.
- 444 2) The draft of downstream box has the significant influence on the wave response around the resonant fre-  
445 quency. With the increase of downstream box draft, the increase of wave response and energy dissipation  
446 can be observed, which is mainly supported by the energy from the upstream box of the two-box system.  
447 It physically expresses the decrease of reflection coefficient with the increase of downstream box draft.
- 448 3) When the draft of downstream box is smaller than that of upstream box, stronger shielding effect can be  
449 observed with the increase of upstream box draft. If the draft of downstream box is larger than that of  
450 upstream box, the increasing reflection coefficient and energy coefficient can be observed with the increase  
451 of upstream box draft, because of the enhanced wave reflection.
- 452 4) With the increase of gap breadth, more energy is required to excite the large-amplitude piston-type of  
453 fluid oscillation as more resonant fluid exists in the narrow gap, which leads to the decrease of reflection  
454 coefficient, and the increase of transmission coefficient. More energy dissipation also happens due to the  
455 fact that more fluid oscillates in the narrow gap with the increase of gap breadth.
- 456 5) For the small upstream and large downstream box drafts, the energy dissipation in the narrow gap is  
457 dominant, resulting in that the wave response in the narrow gap by viscous flow model is smaller than  
458 that by potential flow model. As for the large upstream and small downstream box drafts, the wave  
459 response in the narrow gap by the viscous flow model are always larger than that by the linear potential  
460 flow model because more wave energy is reflected before entering into the narrow gap. If the difference  
461 between the upstream and downstream box drafts is not large, a combining hydrodynamic behavior of  
462 the previous two typical cases can be observed.
- 463 6) As increasing the incident wave amplitude, the reflection coefficient becomes larger at the resonant fre-  
464 quency, which leads to the decrease of transmission coefficient, relative wave response in the narrow  
465 gap, as well as energy dissipation at the resonant frequency. The energy transformation due to the

466 large-amplitude free surface motion can not be ignored in this situation. When away from the resonant  
467 frequency, smaller reflection coefficient and energy coefficient can be obtained, implying that the energy  
468 dissipation becomes the dominant factor for the decrease of wave response in the narrow gap with the  
469 increase of incident wave amplitude.

## 470 **Acknowledgement**

471 This work was supported by the Natural Science Foundation of China with Grant No. 51490673. The  
472 financial support from the Petro China Innovation Foundation with contract No. 2016D-5007-0601 is also  
473 acknowledged. The authors acknowledge the Supercomputer Center of Dalian University of Technology for  
474 providing computing resources.

## 475 **References**

- 476 Ananthakrishnan, P. (2015). Viscosity and nonlinearity effects on the forces and waves generated by a floating  
477 twin hull under heave oscillation, *Applied Ocean Research* **51**: 138–152.
- 478 Berberović, E., van Hinsberg, N. P., Jakirlić, S., Roisman, I. V. and Tropea, C. (2009). Drop impact onto a  
479 liquid layer of finite thickness: Dynamics of the cavity evolution, *Physical Review E* **79**(3): 036306.
- 480 Chen, X.-B. (2004). Hydrodynamics in offshore and naval applications, *Keynote lecture in the 6th Interna-*  
481 *tional conference of Hydrodynamics, Perth, Australia.*
- 482 Elie, B., Reliquet, G., Guillerm, P.-E., Thilleul, O., Ferrant, P., Gentaz, L. and Ledoux, A. (2013). Simulation  
483 of the gap resonance between two rectangular barges in regular waves by a free surface viscous flow solver,  
484 *The 32nd International Conference on Ocean, Offshore and Arctic Engineering (OMAE), Nantes, France.*
- 485 Engsig-Karup, A. P. (2006). *Unstructured nodal DG-FEM solution of high-order boussinesq-type equations*,  
486 PhD thesis, Technical University of Denmark.
- 487 Faltinsen, O. M., Rognebakke, O. F. and Timokha, A. N. (2007). Two-dimensional resonant piston-like  
488 sloshing in a moonpool, *Journal of Fluid Mechanics* **575**: 359–397.
- 489 Faltinsen, O. and Timokha, A. (2015). On damping of two-dimensional piston-mode sloshing in a rectangular  
490 moonpool under forced heave motions, *Journal of Fluid Mechanics* **772**: R1.
- 491 Feng, X. and Bai, W. (2015). Wave resonances in a narrow gap between two barges using fully nonlinear  
492 numerical simulation, *Applied Ocean Research* **50**: 119–129.
- 493 Fredriksen, A. G., Kristiansen, T. and Faltinsen, O. M. (2014). Experimental and numerical investigation of  
494 wave resonance in moonpools at low forward speed, *Applied Ocean Research* **47**: 28–46.

- 495 Fuhrman, D. R., Madsen, P. A. and Bingham, H. B. (2006). Numerical simulation of lowest-order short-  
496 crested wave instabilities, *Journal of Fluid Mechanics* **563**: 415–441.
- 497 Hirt, C. W. and Nichols, B. D. (1981). Volume of fluid (vof) method for the dynamics of free boundaries,  
498 *Journal of computational physics* **39**(1): 201–225.
- 499 Issa, R. I. (1986). Solution of the implicitly discretised fluid flow equations by operator-splitting, *Journal of*  
500 *computational physics* **62**(1): 40–65.
- 501 Iwata, H., Saitoh, T. and Miao, G. (2007). Fluid resonance in narrow gaps of very large floating structure  
502 composed of rectangular modules, *Proceedings of the Fourth International Conference on Asian and Pacific*  
503 *Coasts, Nanjing, China*, pp. 815–826.
- 504 Jacobsen, N. G., Fuhrman, D. R. and Fredsøe, J. (2012). A wave generation toolbox for the open-source cfd  
505 library: Openfoam®, *International Journal for Numerical Methods in Fluids* **70**(9): 1073–1088.
- 506 Jasak, H. (1996). *Error analysis and estimation for the finite volume method with applications to fluid flows*,  
507 PhD thesis, Imperial College London (University of London).
- 508 Jean-Robert, F., Naciri, M. and Chen, X.-B. (2006). Hydrodynamics of two side-by-side vessels experiments  
509 and numerical simulations, *The Sixteenth International Offshore and Polar Engineering Conference, San*  
510 *Francisco, USA*.
- 511 Kristiansen, T. and Faltinsen, O. M. (2010). A two-dimensional numerical and experimental study of resonant  
512 coupled ship and piston-mode motion, *Applied Ocean Research* **32**(2): 158–176.
- 513 Kristiansen, T. and Faltinsen, O. M. (2012). Gap resonance analyzed by a new domain-decomposition method  
514 combining potential and viscous flow draft, *Applied Ocean Research* **34**: 198–208.
- 515 Lu, L. and Chen, X.-B. (2012). Dissipation in the gap resonance between two bodies, *The 27th International*  
516 *Workshop on Water Waves and Floating Bodies, Copenhagen, Denmark*.
- 517 Lu, L., Cheng, L., Teng, B. and Zhao, M. (2010). Numerical investigation of fluid resonance in two narrow  
518 gaps of three identical rectangular structures, *Applied Ocean Research* **32**(2): 177–190.
- 519 Lu, L., Teng, B., Cheng, L., Sun, L. and Chen, X. (2011). Modelling of multi-bodies in close proximity  
520 under water waves-fluid resonance in narrow gaps, *Science China Physics, Mechanics and Astronomy*  
521 **54**(1): 16–25.
- 522 Lu, L., Teng, B., Sun, L. and Chen, B. (2011). Modelling of multi-bodies in close proximity under water  
523 waves-fluid forces on floating bodies, *Ocean Engineering* **38**(13): 1403–1416.
- 524 Mayer, S., Garapon, A., Sørensen, L. et al. (1998). A fractional step method for unsteady free-surface flow  
525 with applications to non-linear wave dynamics, *International Journal for Numerical Methods in Fluids*  
526 **28**(2): 293–315.

- 527 Molin, B. (2001). On the piston and sloshing modes in moonpools, *Journal of Fluid Mechanics* **430**: 27–50.
- 528 Molin, B., Remy, F., Kimmoun, O. and Stassen, Y. (2002). Experimental study of the wave propagation and  
529 decay in a channel through a rigid ice-sheet, *Applied ocean research* **24**(5): 247–260.
- 530 Moradi, N., Zhou, T. and Cheng, L. (2016). Two-dimensional numerical study on the effect of water depth  
531 on resonance behaviour of the fluid trapped between two side-by-side bodies, *Applied Ocean Research*  
532 **58**: 218–231.
- 533 Newman, J. (2004). Progress in wave load computations on offshore structures, *Invited Lecture in The 23rd*  
534 *International Conference on Ocean, Offshore and Arctic Engineering (OMAE), Vancouver, Canada.*
- 535 Rusche, H. (2003). *Computational fluid dynamics of dispersed two-phase flows at high phase fractions*, PhD  
536 thesis, Imperial College London (University of London).
- 537 Saitoh, T. (2007). Private communication.
- 538 Saitoh, T., Miao, G. and Ishida, H. (2006). Theoretical analysis on appearance condition of fluid resonance in  
539 a narrow gap between two modules of very large floating structure, *Proceedings of the Third Asia-Pacific*  
540 *Workshop on Marine Hydrodynamics, Shanghai, China*, pp. 170–175.
- 541 Sun, L., Eatock Taylor, R. and Taylor, P. H. (2010). First-and second-order analysis of resonant waves  
542 between adjacent barges, *Journal of Fluids and Structures* **26**(6): 954–978.